NASA CR-112162

METAL AIRCRAFT STRUCTURAL ELEMENTS REINFORCED WITH GRAPHITE FILAMENTARY COMPOSITES

FINAL REPORT

August 1972

by

K. R. Berg
J. Ramsey

Prepared for

National Aeronautics & Space Administration
Langley Research Center
Hampton, Virginia 23365

Contract No. NAS1-10507

WHITTAKER CORPORATION
Research and Development Division
3540 Aero Court
San Diego, California 92123

FOREWORD

This report was prepared by Whittaker Corporation, Research and Development Division (WRD), San Diego, California, under Contract NAS1-10507, entitled "Metal Aircraft Structural Elements Reinforced with Graphite Filamentary Composites." This program was administered by the National Aeronautics & Space Administration, Langley Research Center, Hampton, Virginia. Mr. Donald Baker was the Project Officer working for the U.S. Army Air Mobility R&D Laboratory at Langley.

Work was conducted at WRD under the general direction of Dr. Kenneth R. Berg, Manager, Structural Development Engineering. James Ramsey served as Principal Investigator.

This report was released for publication on 30 September 1972.

TABLE OF CONTENTS

LIST OF ILLUSTRATIONS

LIST OF ILLUSTRATIONS (Continued)

LIST OF ILLUSTRATIONS (Continued)

LIST OF TABLES

LIST OF SYMBOLS

A_i	cross-sectional area of individual plate elements
a	flange dimension
b	flange dimension, plate width
C_e	coefficient of plate side restraint
E	Young's elastic modulus
E_1	Young's elastic modulus of graphite
E_2	Young's elastic modulus of aluminum
EI	elastic stiffness of combined plate elements
F_{cs}	crippling stress
F_{cy}	compression yield stress
G_a	shear modulus for the adhesive
i	summation subscript
I_{oo}	local inertia of individual plate elements
L	length of panel
N	summation limit
N_x	load per inch of panel
P	load
P_1	load in the graphite
P_2	load in the aluminum
T	temperature
t	thickness
t_1	thickness of the graphite
t_2	thickness of the aluminum
t_a	adhesive thickness
t/b'	effective t/b for a flange

W	weight
x, y, z	local coordinates
y_i	height of neutral axis of individual plate elements from base reference
$\bar{y}$	height of neutral axis of combined plate elements from base reference
α_1, α_2	thermal coefficients of expansion for graphite and aluminum respectively
ϵ_1, ϵ_2	strain in graphite and aluminum respectively
ϵ_{tu}	tensile ultimate strain
ϵ'	additive thermal strain
ν_e	elastic Poisson's ratio
σ_1, σ_2	stress in graphite and aluminum respectively
σ'	additive thermal stress
τ_a	shear stress in the adhesive

METAL AIRCRAFT STRUCTURAL ELEMENTS

REINFORCED WITH GRAPHITE FILAMENTARY COMPOSITES

By K. R. Berg and J. Ramsey

SUMMARY

Strain compatibility equations are used to evaluate the thermal stresses existing when unidirectional graphite composites are bonded to aluminum structures.

Based on thermal stresses and optimum placement of the composite, skin-stringer aluminum panels are optimized for minimum weight compression panels with selective composite reinforcement.

Composite reinforced skin-stringer panels are thermal cycled to determine the effect of thermal fatigue on structural integrity. Both cycled and uncycled panels are tested in compression and tension. Test results are correlated with predicted loads.

Use of filamentary graphite composites are an efficient method of reinforcing metal structures, but care must be taken to minimize thermal stresses.

INTRODUCTION

The use of advanced composites for reinforcing aluminum structures has been proven effective by NASA in both in-house and contracted programs. The work has primarily been conducted using boron and graphite fibers as the composite reinforcement. Since graphite appears to have a much greater potential as a lower cost material, it is desirable to determine the efficiency of graphite composite material as a reinforcement for aluminum structures.

A program was therefore undertaken involving the study of the use of composites for reinforcing an aluminum skin stringer panel by bonding unidirectional graphite epoxy laminates to selective areas of the panel. This report summarizes that program. It was conducted by Whittaker Corporation, Research & Development Division (WRD) for Langley Research Center of NASA under Contract NAS 1-10507.

The program to develop a composite reinforced skin-stringer panel included the following:

- Analysis of the thermal stresses that are generated due to the differences in thermal coefficients for the aluminum and the graphite composite material.

- Selection of optimum materials for construction of the reinforced panels. This includes the selection of the adhesive, the graphite fiber, and the matrix for the graphite composite.

- Optimization of the reinforced skin-stringer panel which includes the determination of the geometry of the panel, and the amount and location of the graphite composite reinforcement based on the program requirement that panels be designed to carry 1/2 and 1/3 of the total load in the graphite epoxy.

- Analysis of the resultant optimum panel configurations including the prediction of the load carrying capability of the panels in tension and compression.

- Fabrication of the test panels. This involves the utilization of both 2024-T3 and 7075-T6 aluminum sheet and stringers. Unidirectional graphite composite strips were bonded to the inner side of the crown of the hat and to the skins. The hats were riveted to the skin.

- Testing of the panels in compression and tension, before and after thermal cycling.

- Correlation of the predicted loads and test data, and efficiency of the graphite reinforced aluminum panel.

The use of fibrous composites for reinforcing metals has shown significant weight savings over all metal structures. A proper design is necessary to account for thermal stresses.

The following sections contain a description of the thermal analysis, material selection, panel optimization, fabrication of panels, testing program, and the conclusions.

THERMAL ANALYSIS

Advanced composite - metal systems pose new problems of material compatibility. Due to the significant differences of thermal behavior of the constituent materials it was deemed necessary that an investigation of the thermal behavior of the combined system be undertaken.

Since the composite system under consideration is one of long narrow strips of graphite bonded to aluminum, the effect of the difference in coefficients of expansion will be most important in the longitudinal direction. Thus it is sufficient to consider only elastic, one dimensional deformation. Furthermore, the model is considered to be constrained to deform only in its original plane.

Consider the following composite strip model (Figure 1)

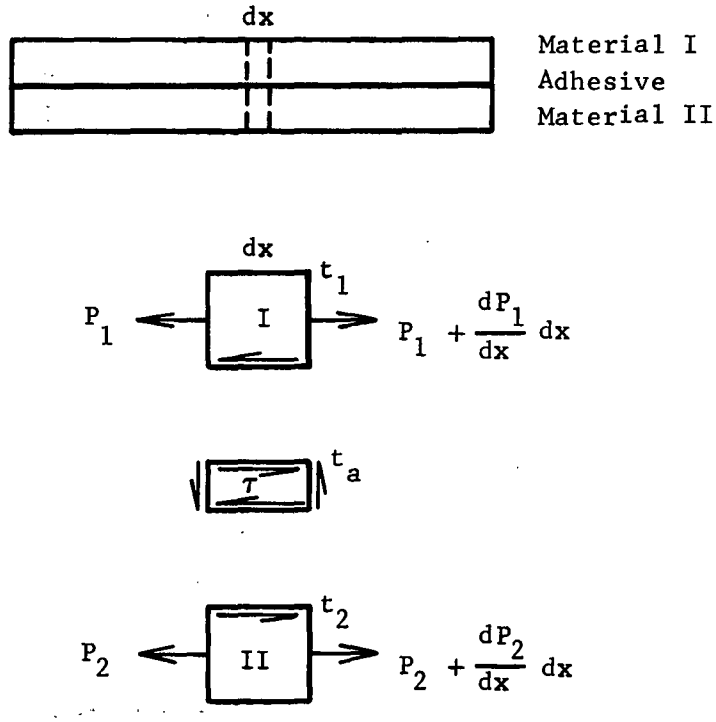

Figure 1. Composite Strip Model.

For equilibrium

$$\tau \cdot b - \frac{dP_1}{dx} = 0 \tag{1}$$

$$\tau \cdot b + \frac{dP_2}{dx} = 0 \tag{2}$$

Taking into account the relationship between the thermally induced strains in the adherends and the shear strain in the adhesive, the following differential equation results:

$$\frac{d^2\tau(x)}{dx^2} = \frac{1}{b} \cdot \frac{dP_1(x)}{dx} \cdot \frac{G_a}{t_a} \cdot \left(\frac{1}{E_1 \cdot t_1} + \frac{1}{E_2 \cdot t_2} \right) \tag{3}$$

or from (1)

$$\frac{d^2\tau(x)}{dx^2} - k^2 \cdot \tau(x) = 0 \tag{4}$$

where

$$k^2 = \frac{G_a}{t_a} \cdot \left(\frac{1}{E_1 \cdot t_1} + \frac{1}{E_2 \cdot t_2} \right) \tag{5}$$

The coordinates for the deformation have been selected so that deformation is symmetrical with regard to the y-axis (see Figure 2)

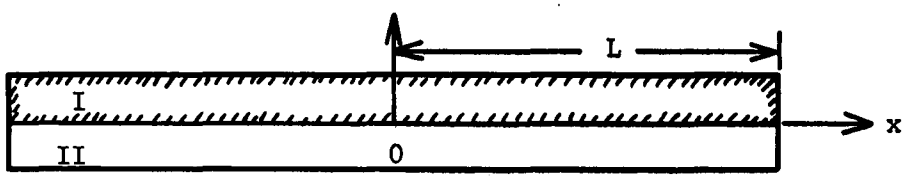

Figure 2. Composite Strip Model.

Thus at x=0 the shear strain in the adhesive must be zero. Furthermore, since all deformation is thermally induced, the load carried by the end faces of the model must be identically equal to zero.

$$P_1(L) = P_2(L) = 0 \tag{6}$$

With these boundary conditions in mind, a relationship for $\tau(x)$ follows immediately.

$$\tau(x) = \frac{G_a \cdot (\alpha_1 - \alpha_2) \cdot \Delta T \cdot \sinh kx}{t_a \cdot k \cdot \cosh kL} \tag{7}$$

Referring to (1) and integrating through the limits of x to L results in

$$\sigma_1(x) = - \frac{G_a \cdot (\alpha_1 - \alpha_2) \cdot \Delta T \cdot (\cosh kL - \cosh kx)}{k^2 \cdot t_a \cdot t_1 \cdot \cosh kL} \tag{8}$$

$$\sigma_2(x) = + \frac{G_a \cdot \left(\alpha_1 - \alpha_2\right) \cdot \Delta T \cdot (\cosh kL - \cosh kx)}{k^2 \cdot t_a \cdot t_2 \cdot \cosh kL} \tag{9}$$

σ_1 and σ_2 reach a maximum at $x=0$. Introducing an appropriate substitution from (5) and observing that $\cosh kL \gg 1$ results in

$$\sigma_{1\ max} = - \frac{\left(\alpha_1 - \alpha_2\right) \cdot \Delta T \cdot E_1 \cdot E_2 \cdot t_2}{E_1 \cdot t_1 + E_2 \cdot t_2} \tag{10}$$

$$\sigma_{2\ max} = \frac{\left(\alpha_1 - \alpha_2\right) \Delta T \cdot E_1 \cdot E_2 \cdot t_1}{E_1 \cdot t_1 + E_2 \cdot t_2} \tag{11}$$

Allowing strip I to be unidirectional graphite and strip II to be aluminum, a substitution of appropriate material constants and dimensions results in the stress distributions presented in Figure 3.

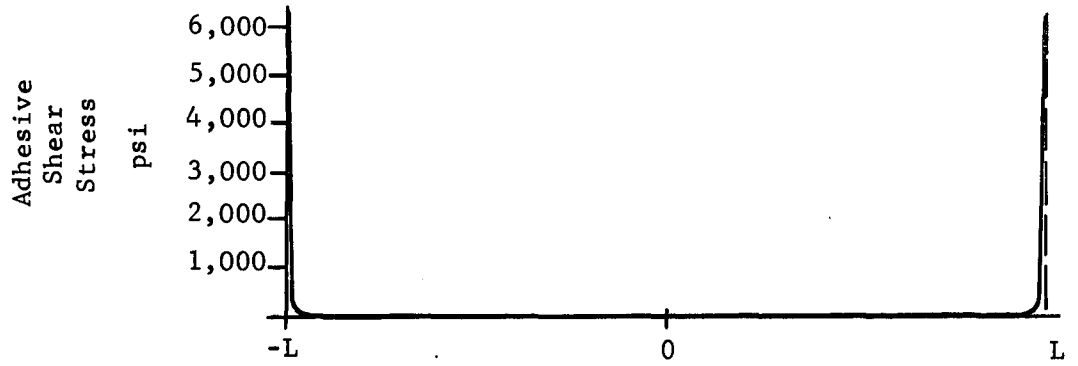

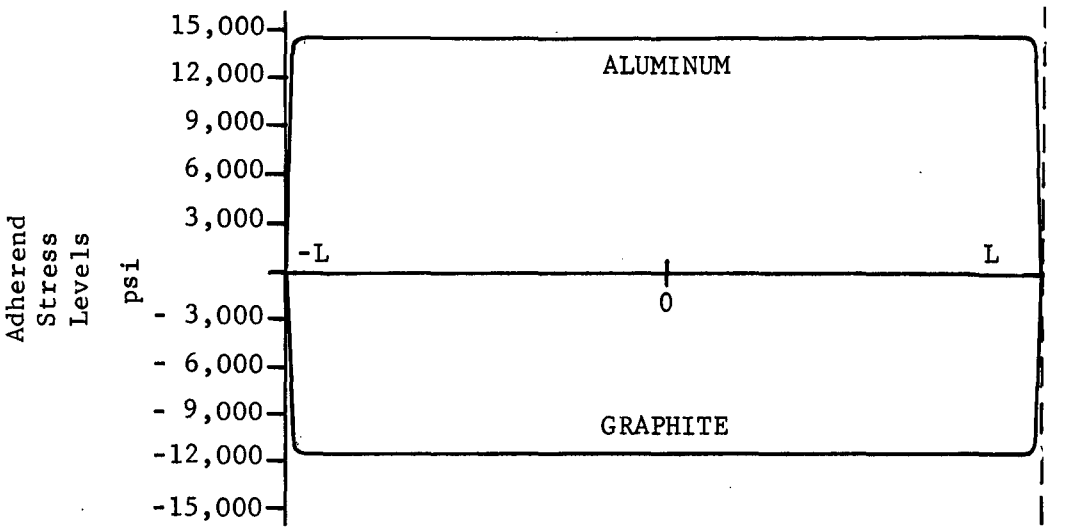

$\alpha_1 = -.4 \times 10^{-6} \frac{in}{in\text{-}F^\circ}$

$\alpha_2 = 12 \times 10^{-6} \frac{in}{in\text{-}F^\circ}$

$G_{Adhesive}$ = 120,000 psi Adhesive Thickness = .003

$t_{Graphite}$ = .030 inch

$t_{Aluminum}$ = .025 inch

ΔT = -150F°

Figure 3. Typical Thermal Stress Levels.

MATERIALS SELECTION

Discussion of Candidate Graphite Fibers

The more common high tensile strength and high tensile modulus graphite fibers are listed in Tables I and II. For this program a high tensile strength graphite fiber was selected as the primary evaluation fiber as a result of indications that the use of higher modulus fibers produce significantly higher thermal stresses. However, a limited number of panels were fabricated utilizing the high modulus fiber for comparison purposes. As can be seen from the properties of the high tensile strength graphite fibers in Table I the range in strength and modulus is quite narrow and thus selection of any of these manufacturers would be acceptable. Based on the ease of obtaining fibers from one of our own divisions and its competitive price, the Whittaker-Morgan Modmor Type II fiber was selected.

For the high modulus fiber the range in modulus is significantly greater as shown in Table II. However, as a demonstration of the differences that fiber modulus contribute, the Whittaker-Morgan Modmor Type I fiber was chosen. The reason again being availability, cost, and a good representative high modulus fiber.

TABLE I. — PROPERTIES OF A SELECTED NUMBER OF HIGH TENSILE STRENGTH GRAPHITE FIBERS

Manufacturer	Identification	Tensile Strength, 10^3 psi	Tensile Modulus, 10^6 psi	Specific Gravity, g/cm^3
Union Carbide	Thornel 400	425	30	1.78
Great Lakes Carbon	Fortafil 3T	200	28	1.7
Great Lakes Carbon	Fortafil 4T	350	37	1.7
Hercules	Type A	300	30	1.75
Hercules	Type HT-S	350	35	1.76
Whittaker-Morgan	Type II	375	40	1.7

TABLE II. — PROPERTIES OF A SELECTED NUMBER OF HIGH TENSILE MODULUS GRAPHITE FIBERS

Manufacturer	Identification	Tensile Strength, 10^3 psi	Tensile Modulus, 10^6 psi	Specific Gravity, g/cm^3
Union Carbide	Thornel 50S	270	57	1.67
Union Carbide	Thornel 75S	360	76	1.82
Great Lakes Carbon	Fortafil 5T	400	48	1.8
Great Lakes Carbon	Fortafil 6T	420	59	1.9
Hercules	Type HM-S	300	55	1.92
Whittaker-Morgan	Type I	400	65	2.00
Celanese	GY-70	300	88	1.96

Discussion of Candidate Matrix Systems

The selection of a matrix system is not primarily based on its mechanical properties but rather on such considerations as viscosity, flow, shelf life, handleability, etc... Many resin systems have been used with graphite fibers with the best results being obtained from structural epoxy resins. Analytically (and actually) the matrix contribution to graphite/epoxy laminate properties due to its mechanical properties is not significant. It appears that variations in strength (and to a lesser extent modulus) are due to a much larger degree to process variations, care in collimation, and resin physical characteristics (flow, etc.) rather than the selection of a specific mechanical property in the resin. Thus, the utilization of a given resin system is actually based on processing procedures which permit that resin to provide acceptable properties when fabricated into a graphite composite. As an example, Union Carbide 4617, an epoxy resin, has been used in conjunction with many different graphite fibers and depending on the fabrication processes used differences in properties result. For example, in comparing a Great Lakes Carbon fiber and a Hercules fiber (Courtalds) better flexural and tensile properties resulted for the Great Lakes fiber but lesser compressive properties.

In like manner the properties of high modulus graphite fibers utilizing 4617 resin system also produced scattered results as shown in Table IV. Again, the variation in the mechanical properties of the resin system itself produces less of a variable factor than does the processing.

The 4617 resin system would not necessarily produce the maximum properties but it would provide good properties in most applications. In addition, the 4617 resin system is commercially available, relatively low cost, is highly workable in fabrication, and provides quite acceptable repetitive properties and was thus selected.

The basic properties for the selected systems, Modmor I and II with the 4617 resin system are shown on Tables III and IV.

TABLE III. – MECHANICAL PROPERTIES OF UNIDIRECTIONAL EPOXY RESIN COMPOSITES WITH A SELECTED NUMBER OF HIGH TENSILE STRENGTH GRAPHITE FIBERS

Fiber	Resin	Flexural Strength, 10^3 psi	Flexural Modulus, 10^6 psi	Tensile Strength, 10^3 psi	Tensile Modulus, 10^6 psi	Compression Strength, 10^3 psi	Compression Modulus, 10^6 psi	Short Beam Shear, 10^3 psi
II	4617/MDA	220	19	170	20	160	20.0	15.5
4T	4617/MDA[1]	200	20	170	-	160	-	14
A	X-19[2]	202	16	208	23	148	22	8.7
HT-S	4617/m-PDA[3]	163	18	143	19	167	21	16.5
II	1004[4]	250	20	180	22	160	-	16

Source of Date: (1) Great Lakes Carbon
(2) Fiberite Corp.
(3) Hercules, Inc.
(4) Narmco

TABLE IV. — MECHANICAL PROPERTIES OF UNIDIRECTIONAL EPOXY RESIN COMPOSITES WITH A SELECTED NUMBER OF HIGH TENSILE MODULUS GRAPHITE FIBERS

Fiber	Resin	Flexural Strength, 10^3 psi	Flexural Modulus, 10^6 psi	Tensile Strength, 10^3 psi	Tensile Modulus, 10^6 psi	Compression Strength, 10^3 psi	Compression Modulus, 10^6 psi	Short Beam Shear, 10^3 psi
50S	4617 (1)	137	32	148	33	100	33	8
I	4617 (1)	160	31	140	32	127	29	9
5T	4617/MDA (2)	220	25	170	-	150	-	11
6T	4617/MDA (2)	170	30	150	-	120	-	9
HMS	3002 (3)	138	27	102	26	117	-	10.5
I	1004 (4)	145	32	120	33	112	-	9
GY-70	350A (5)	115	37	90	42	90	-	9

Source of Data:
(1) Union Carbide
(2) Great Lakes Carbon
(3) Hercules, Inc.
(4) Narmco
(5) Celanese

Discussion of Candidate Adhesive Systems

The bonding of graphite composite material to aluminum substrates can be performed in two manners: cocuring or secondary bonding. The cocuring approach can be performed in two manners; first, the matrix system in the uncured composite material can be used as the adhesive and second, an adhesive system with compatible cure schedules can be cured simultaneously with the composite material. The secondary bonding approach is one wherein the composite adherend is precured and later bonded to the aluminum substrate.

The problem of minimizing the warpage resulting from the mismatch of thermal expansion between the graphite composite and the aluminum substrate is related to the bonding temperature, the thickness of the adhesive glue line and the stiffness properties of the adhesive material. In some respects the orientation of the graphite composite will contribute significantly to the thermal expansion mismatch. However, the degree to which the bonded panel warps is still a function of the three items mentioned above for any given ply orientation.

The worst case condition for warpage due to differential thermal expansion is the cocuring technique wherein the matrix system is used as the adhesive and the assembly is cured at high temperatures (see Figures 4 and 5). The residual stress developed in the cool-down phase of the cure cycle is intimately transferred to the two adherends. Assuming the cure temperatures are identical, the second worst case is a cocuring technique using an adhesive layer between the composite and the aluminum (see Figures 6 and 7). The adhesive, having isotropic thermal expansion properties and being of lower modulus than the graphite adherend, will tend to dissipate and absorb a portion of this stress proportional to its thickness. The thicker the glue line, the more capacity for stress distribution. If the cure temperatures were lowered (and adequate cures could be obtained) a lesser degree of warpage would result.

A further reduction in warpage is possible if the graphite composite adherend is precured and secondarily bonded to the aluminum substrate (see Figures 8 and 9). This assumes the use of the same adhesive as was used in the second case of cocuring procedures. The lower stress condition is obtained because the cured graphite composite has thermal expansion properties, whereas in the cocured method it has no expansion properties until after it has been cured at the elevated temperature. Therefore, the degree of improvement obtained is proportional to the elongation that the graphite composite undergoes during the bonding cycle. As discussed above, further improvements can be made by lowering the adhesive cure temperature and using a thicker glue line.

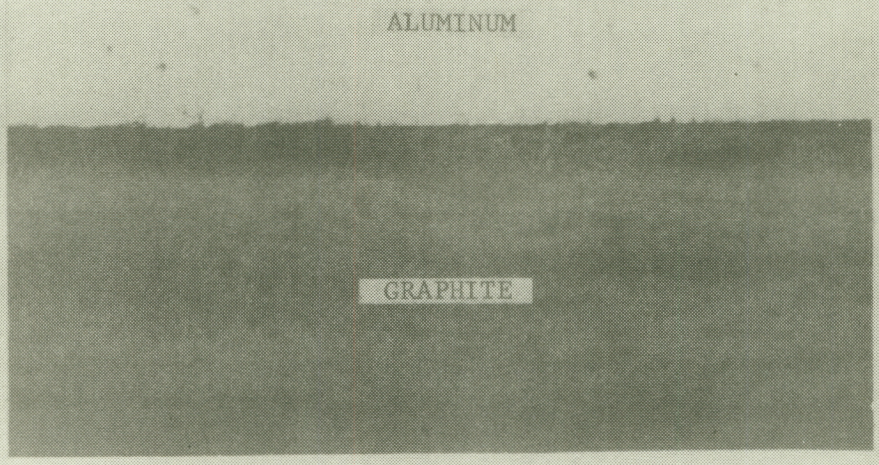

Figure 4. Cocure Without Adhesive-Magnification 44x.

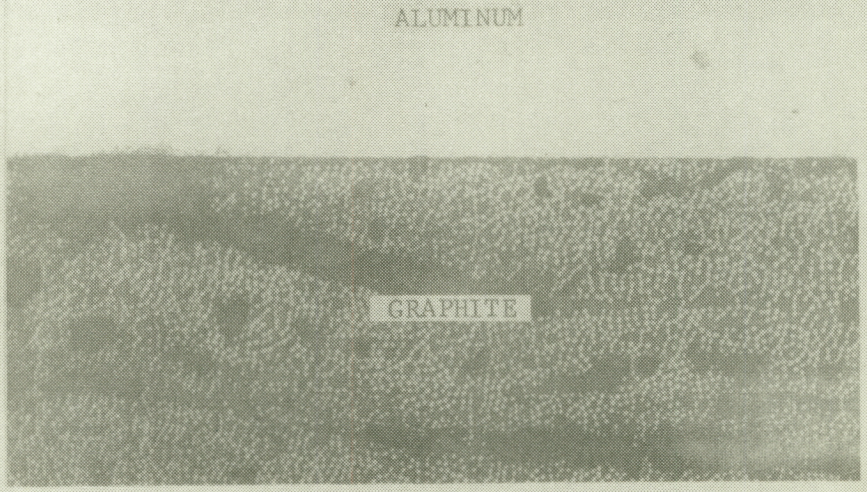

Figure 5. Cocure Without Adhesive-Magnification 88x.

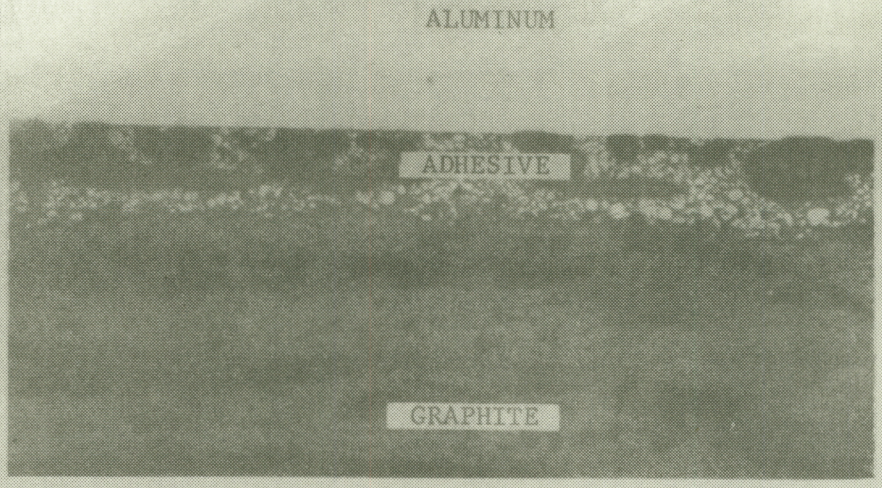

Figure 6. Cocure With Adhesive-Magnification 44x.

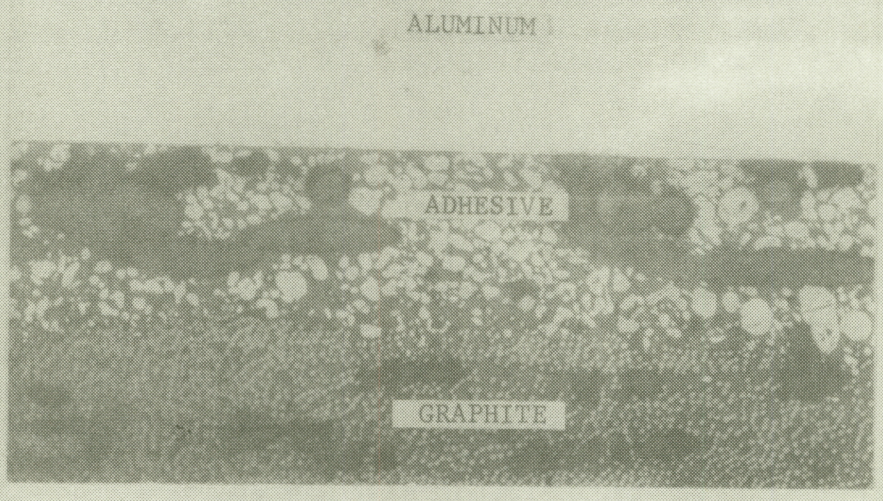

Figure 7. Cocure With Adhesive-Magnification 88x.

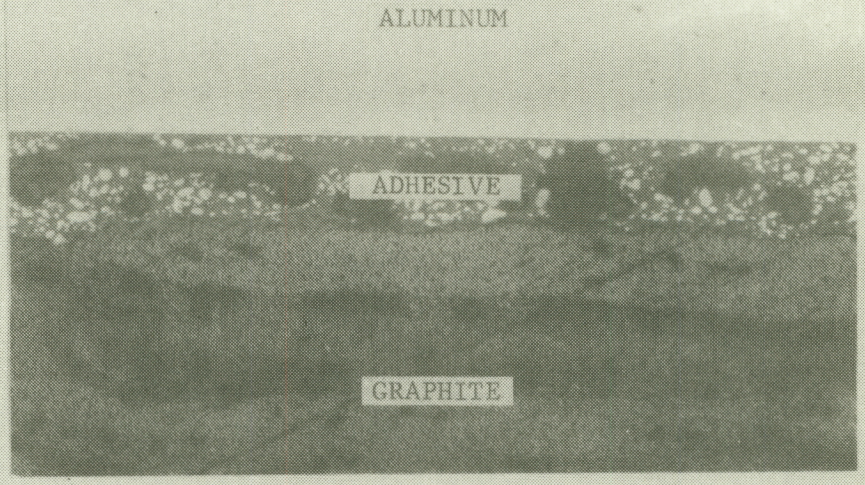

Figure 8. Secondary Bond-Magnification 44x.

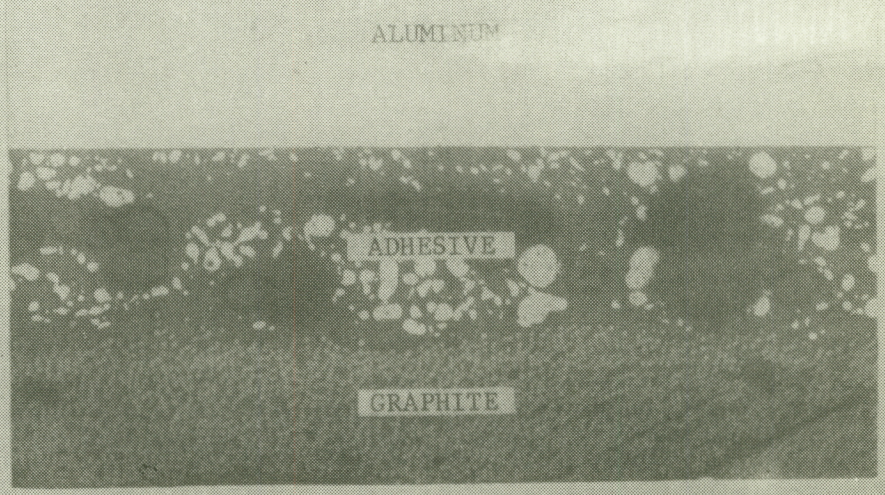

Figure 9. Secondary Bond-Magnification 88x.

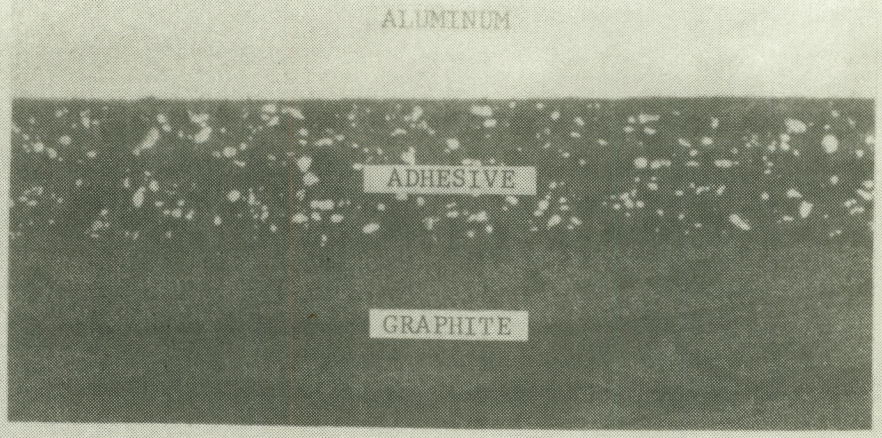

Figure 10. Secondary Bond-Room Temperature Cure-Magnification 44x.

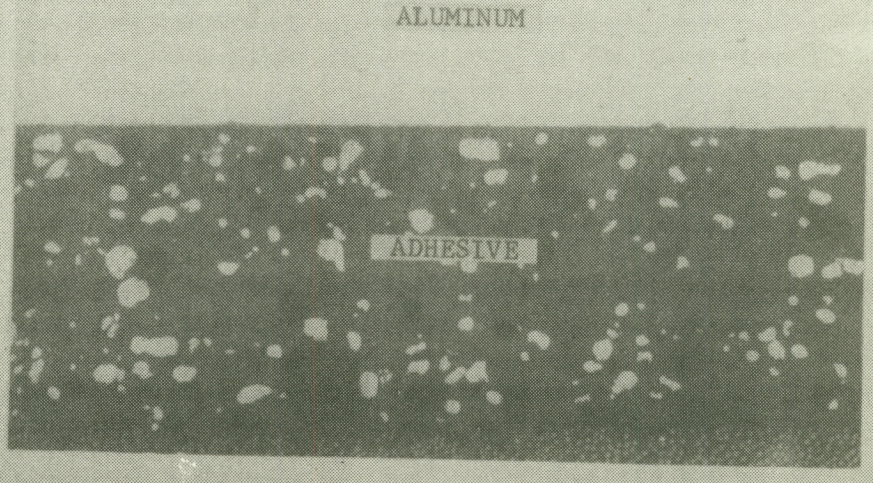

Figure 11. Secondary Bond-Room Temperature Cure-Magnification 88x.

The least amount of warpage is obtained by secondarily bonding the aluminum to a cured graphite composite using a room temperature cure adhesive (see Figures 10 and 11). Any significant warpage resulting from the room temperature cure can be attributed to the shrinkage of the adhesive system when it cures.

The following is a discussion of candidate adhesive systems which have been determined to be suitable for bonding graphite to aluminum substrates.

1. Metlbond 329 — Metlbond 329 is a modified epoxy containing aluminum powder as a filler. The adhesive is available in a film form having a synthetic fabric carrier. The material possesses excellent bonding characteristics to both aluminum and graphite and maintains a high strength level up to approximately 400°F. While the material can be cured under various temperature conditions and at different time intervals, the lowest temperature to achieve a satisfactory cure is 275°F. Thus, while this adhesive system provides excellent properties, considerable stress will be developed at the glue line due to the elevated temperature cures. In comparing this material to other candidate adhesive systems it would be considered to have a higher modulus and lower elongation and tend to transfer residual stress rather than absorb any significant portion.

2. Metlbond 225 — Metlbond 225 is a low temperature curing elastomer modified epoxy adhesive supported on a non-woven synthetic fabric carrier. This material can be cured at temperatures as low as 200°F or for optimum cures for short periods of time, up to 225°F. Material is available in various thicknesses ranging up to 15 mils thick.

   Metlbond 225 exhibits good shear strength from -67° up to a useful temperature of 180°F. It has a maximum elevated temperature use of 250°F. Room temperature strengths for this material in lap shear on aluminum is in excess of 4,000 psi. It maintains this value up through 180°.

   The degree of warpage obtained with the Metlbond 225 material would be considerably less than the above mentioned Metlbond 329, primarily because of its lower cure temperature. However, combined with the low cure temperature is the fact that the 225 system contains an elastomeric phase which will absorb and distribute a major portion of the stress. Since this material can be obtained in various thicknesses, one would be able to optimize the thickness which would also result in a net reduction in warpage.

Unless the matrix system for the graphite/epoxy composite also cures at 200-225°F the Metlbond 225 is not applicable for cocuring purposes.

3. Adhesive EA934 (formerly Shell Epon Adhesive 934) – The 934 adhesive consists of a two-part adhesive system containing aluminum powder as a filler. The 934 system is a room temperature curing system that takes several days to cure, but yields shear strengths of 3,000 psi at room temperature and in excess of 2,000 psi at 180°F. When cured at room temperature this system would provide essentially zero warpage when bonding aluminum and graphite adherends.

The three adhesive systems mentioned above are typical of many adhesive systems which fall into the three classes, namely elevated temperature cures, moderate elevated temperature cures, and room temperature cures. These systems are not normally available in thickness over about 15 mils; however, the effect of glue line thickness on residual stress and radius of curvature developed between the aluminum and graphite composite can be established by using multiple layers of adhesive film to bond the composite.

In order to determine the effect of thermal cycling on adhesive systems a number of tests were performed. The test specimen was a simple lap shear specimen, with aluminum bonded to unidirectional graphite/epoxy laminate. Both 2024-T3 and 7075-T6 aluminum were utilized. Metlbond 225 cured at 225°F and 350°F was utilized as well as Epon 934, a room temperature cure adhesive. Cocuring techniques and secondary bond techniques were both utilized. The thermal cycling consisted of 500 cycles from -60° to +160°F. Based on the limited testing conducted, test results indicated retention in static strength of from 44 to 120%. Lap shear strengths and percent strength retention data for all of the specimens tested are shown on Tables V and VI.

As a result of this test program the cure temperature for Metlbond 225 of 225°F was selected. The procedure utilizing precured graphite/epoxy and secondary bonding to the aluminum was selected as the method of fabrication. The results of the tests for this approach (see Table VI) indicate only a 14% loss in strength due to thermal cycling.

It is apparent from the above discussion that the room temperature cure is the best of the candidate systems if it meets the loading requirements. However 3,000 psi shear strength for the tensile loading case may be marginal. In addition, room temperature cure adhesives at present exhibit an unfortunate degree of degradation with environments and aging. Thus the most reasonable choice for strength and minimum warpage is the Metlbond 225 system.

TABLE V. – EFFECT OF 500 CYCLES OF THERMAL ENVIRONMENT OF STRENGTH OF LAP SHEAR SPECIMENS

Specimen Identification	Description	Strength Before Cycling (psi)	Strength After Cycling (psi)	% Strength Retention After Thermal Cycling
A-11-1	Co-Cure	1440		
A-11-2	No Adhesive	1470		44
A-11-3	7075-T6		641	
A-12-1	Co-Cure	1310		
A-12-2	No Adhesive	1260		74
A-12-3	2024-T3		946	
C-11-1		3770		
C-11-2	Co-Cure	3780		62
C-11-3	Adhesive		2320	
C-12-1	Metlbond 225	3300		
C-12-2	(Cure 350°F)	3440		75
C-12-3			2540	
F-11-1		3780		
F-11-2		3960		47
F-11-3	Secondary Bond		1820	
F-12-1	Metlbond 225 (Cure 225°F)	2590		
F-12-2		3870		56
F-12-3			1800	
G-11-1	Secondary Bond	2060		
G-11-2	Metlbond 225	1790		60
G-11-3	(Cure 250°F) Modmor I		1160	
H-11-1	Secondary	1462		
H-11-2	R.T. Cure	1900		122
H-11-3			2060	

TABLE VI. – EFFECT OF 500 CYCLES OF THERMAL (-60°F TO 160°F) ENVIRONMENT ON STRENGTH OF LAP SHEAR SPECIMENS

Specimen Identification	Description	Strength (psi) Without Cycling	After Cycling	% Strength Retention After Thermal Cycling
C-12-4	Co-Cure	2370		
	No Adhesive	2890		
	2024-T3	2930		
C-12-7	Co-Cure		2590	72*
C-12-8	No Adhesive		1320	73**
C-12-9	2024-T3		2080	
F-12-4	Secondary	3640		
F-12-5	Bond	2810		
F-12-6	Metlbond 225	3490		
	Cure 225°F	3310±		
F-12-7	Secondary		3120	
F-12-8	Bond		2770	86*
F-12-9	Metlbond 225		2670±	86.6**

*Based on average to average comparison

**Based on average of high to high, low to low comparisons

±Average

With the basic material properties for the stringer panels now established it is now possible to proceed with a detailed analysis and design of an optimum panel configuration.

PANEL ANALYSIS

The analysis of the hat-shaped skin stiffener poses several interesting problems to the designer. Most if not all of the previous analytical approaches have relied heavily on empirical results. The problem is that several areas of the hat-skin combination, such as the area about the flanges, the rivets and the corners, are stiffer than other areas. No exact method has been found to define the increased stiffness in the skin about the flanges. This increased stiffness appears to be dependent on flange width and thickness, the distance between flanges, the method of flange to skin joining, etc...

The problem is further increased by the addition of an advanced composite such as graphite to the inner surface of the hat and the skin, thus introducing new areas of increased stiffness. Perhaps the easiest approach to the problem is to analytically divide the hat-skin combination into sections that lend themselves to easy analysis. Although the variety of means by which this may be done is almost endless, a suggested model is presented in Figure 12.

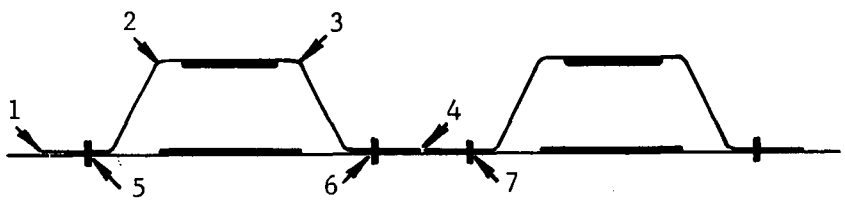

Figure 12. Stringer Model.

The aluminum panel between points 6 and 7 was treated as a simple panel with pinned side supports. The buckling formula for this section is

$$\sigma_{cc} = \frac{k_s \pi^2 E}{12\left(1-\nu_e^2\right)}\left(\frac{t}{b}\right)^2 \qquad (12)$$

Where k_s is the coefficient of side fixity. The fixity coefficient for pinned side supports is 4.0.

The buckling loads of the angle sections between points 1 and 2 and 3 and 4 were calculated by the Needham angle method (Reference 1).

The Needham angle method computes an effective b''/t based on the dimensions of the angle (see Figure 13).

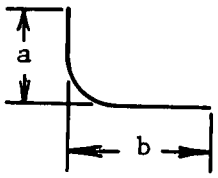

Figure 13. Analytical Angle.

$$b''/t = \frac{a+b}{2t} \tag{13}$$

For a crown width of .75 in. and a hat height of .5 in. the web length will be .625 in.. The flange width is .5 in. wide. Thus

$$b''/t = \frac{a+b}{2t} = \frac{.625 + .5}{2\ (.025)} = 22.5$$

The above angle has three possible end conditions: (1) both ends free; (2) 1 free - 1 fixed; (3) both ends fixed. The crippling stress is found by the following formula:

$$F_{cs}\Big/\left(F_{cy} \cdot E\right)^{\frac{1}{2}} = C_e \cdot \left(\frac{t}{b''}\right)^{\frac{3}{4}} \tag{14}$$

where

F_{cs} = crippling stress (psi)

F_{cy} = compression yield stress (psi)

E = Young's modulus in compression

b''/t = equivalent b/t of section = $(a + b)/2t$

C_e = coefficient that depends on the degree of edge support along the edges of contiguous angle units. Specifically:

Case I: $C_e = 0.316$ — both ends free

Case II: $C_e = 0.342$ — one end free — one end fixed

Case III: $C_e = 0.366$ — both ends fixed

Referring to Figure 14 for the no edges free condition,

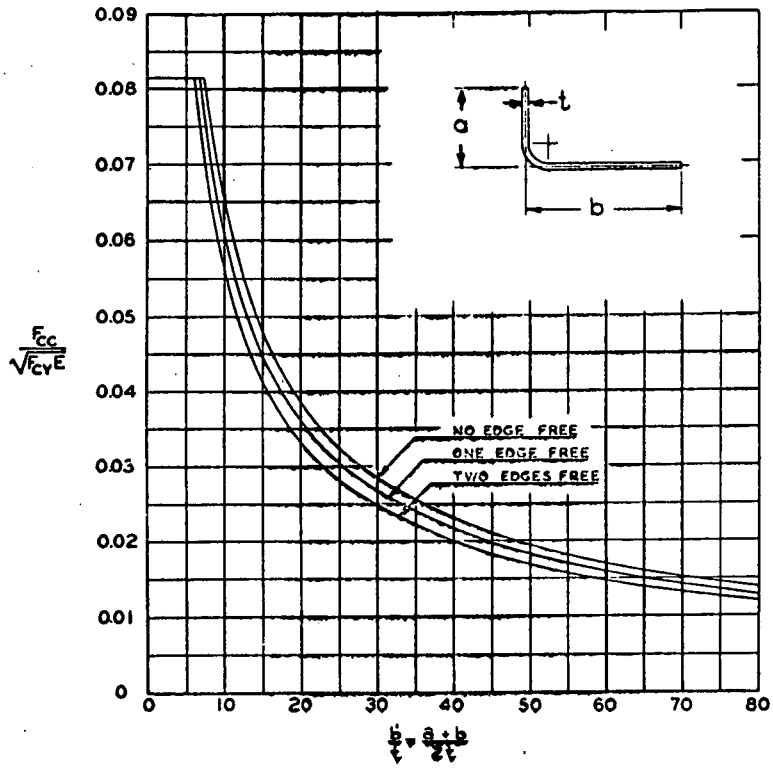

(Note: F_{cc} same as F_{cs})

Figure 14. Dimensionless Crippling Stress vs. b′/t (Reference 1).

$$\frac{F_{cc}}{\left(F_{cy} \cdot E\right)^{\frac{1}{2}}} = .035$$

For 2024-T3 $F_{cy} = 39{,}000$ psi, $E = 10.7 \times 10^6$ psi

$$\left(F_{cy} \cdot E\right)^{\frac{1}{2}} = 6.46 \times 10^5 \text{ psi}$$

$$F_{cc} = .035 \times 6.46 \times 10^5 \text{ psi} = 22{,}610 \text{ psi}$$

This stress is well within the linear-elastic range of 2024-T3. Thus it is expected that the variation of 7075-T6 from this value is negligible. Within the linear-elastic range the buckling stress for 7075-T6 is 22,400 psi.

The buckling of the graphite-aluminum plates (Plates 2-3 and 5-6) takes into account the following considerations.

1. Strain compatibility – limiting graphite strain

2. Composite EI

3. Plasticity of aluminum-effect on composite EI

The graphite-aluminum plates were treated as simple plates with effective neutral axis and EI. The formula for the crippling of panel elements is

$$P_{cc} = \frac{k \cdot EI}{b^2} \tag{15}$$

where

$$k = \frac{k_s \cdot \pi^2}{\left(1-\nu_e^2\right)} \tag{16}$$

k_s = constant of side fixity

For the graphite-aluminum plates the side fixity was set at 4.0. Thus,

$$k = \frac{4.0 \cdot 9.85}{\left(1-(.3)^2\right)} \simeq 43$$

$$EI = \sum_{i=1}^{N} E_i A_i y_i^2 + \sum_{i=1}^{N} E_i I_{ioo} - \sum_{i=1}^{N} E_i A_i \bar{y}^2 \tag{17}$$

where y_i is the distance from baseline reference to the neutral axis of the i^{th} element.

The EI of the graphite-aluminum plate will change with change in the modulus of the aluminum due to plasticity. The effect of this change of EI on the buckling load is plotted in Figures 15, 16, and 17. In addition the strain corresponding to the change in aluminum modulus is used to determine the load as a function of modulus. This function is also plotted in Figures 15, 16 and 17. If the graphs intersect within the range of allowable strain and modulus, then the point of intersection is the buckling load. If the intersection occurs at a modulus value that corresponds to a strain greater than the available strain in the graphite, then the graphite will fail before the panel can buckle. If the intersection occurs at a modulus value greater than the elastic modulus of the aluminum, then the panel will buckle in the elastic range of the aluminum. Figures 15, 16 and 17 present three such plotting calculations for different thicknesses of graphite for element 5-6. Table VII presents a list of buckling loads for various thickness of graphite for element 5-6.

TABLE VII. – BUCKLING LOADS AS A FUNCTION OF GRAPHITE THICKNESS

Aluminum Type	Aluminum Thickness in.	Aluminum Width in.	Modmor II Graphite Width in.	Modmor II Graphite Thickness in.	$P_{Failure}$ lbs	$\epsilon_{Failure}$ in/in
2024-T3	.025	2.0	1.0	.025	2400	Linear
2024-T3	.025	2.0	1.0	.03	3100	Linear
2024-T3	.025	2.0	1.0	.04	4300	.00325
2024-T3	.025	2.0	1.0	.05	5450	.0037
7075-T6	.025	2.0	1.0	.025	2338	Linear
7075-T6	.025	2.0	1.0	.03	3086	Linear
7075-T6	.025	2.0	1.0	.04	5134	Linear
7075-T6	.025	2.0	1.0	.05	7550	.005

Early in the analysis certain parameters were fixed. The flanges of the hat section would have to be about .5 in. wide to facilitate easy riveting. A limit had to be set on the amount of free skin between rivets. Based on classical buckling considerations it was desirable to keep this span within .5 to .75 in. In order to maximize the allowable stress in this region a span of .5 inches was selected. This distance left 2 inches between rivets for the composite section. Actually only 1.5 inches in available surface is left on the hat side of the skin.

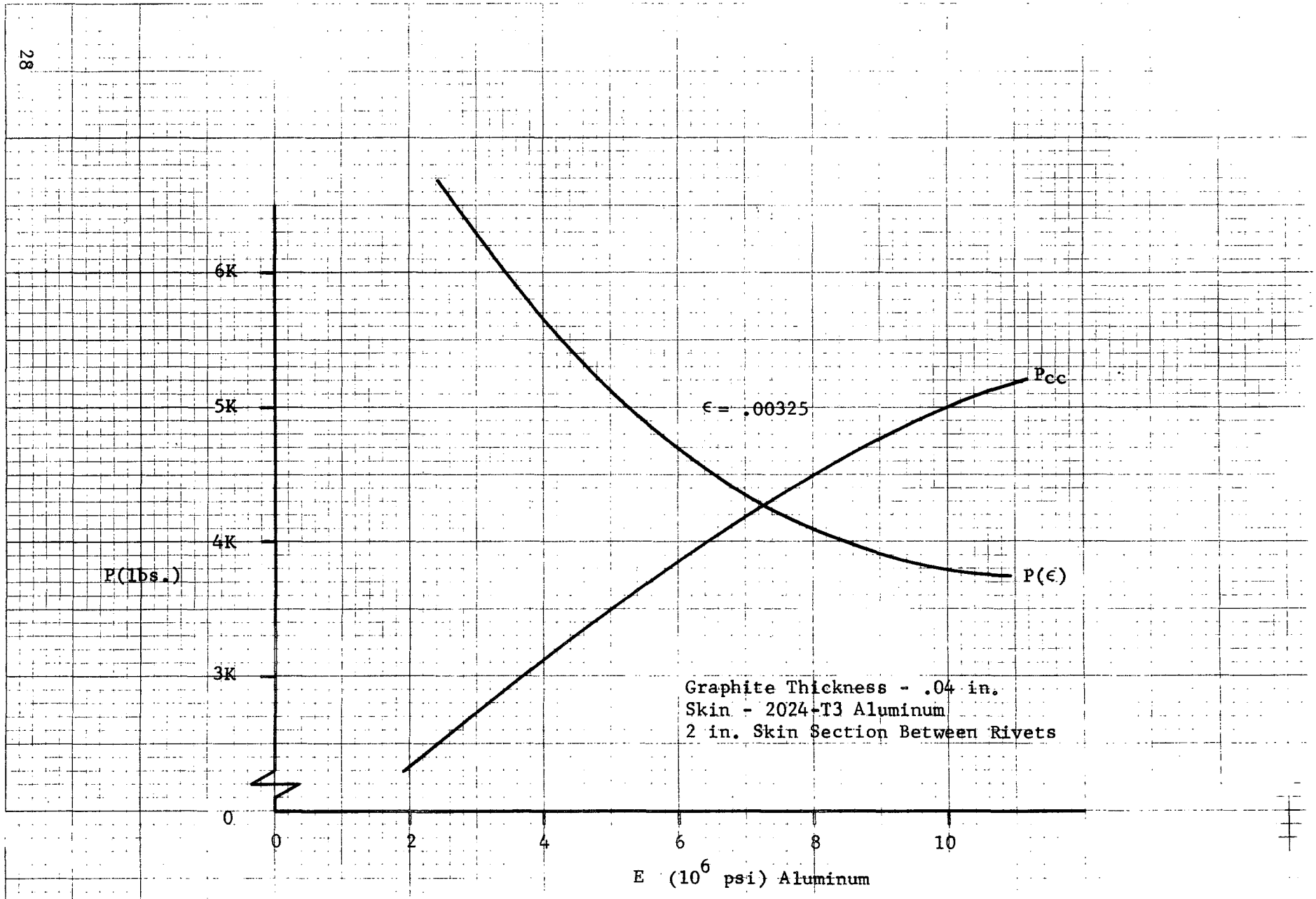

Figure 15. Composite Plate Buckling.

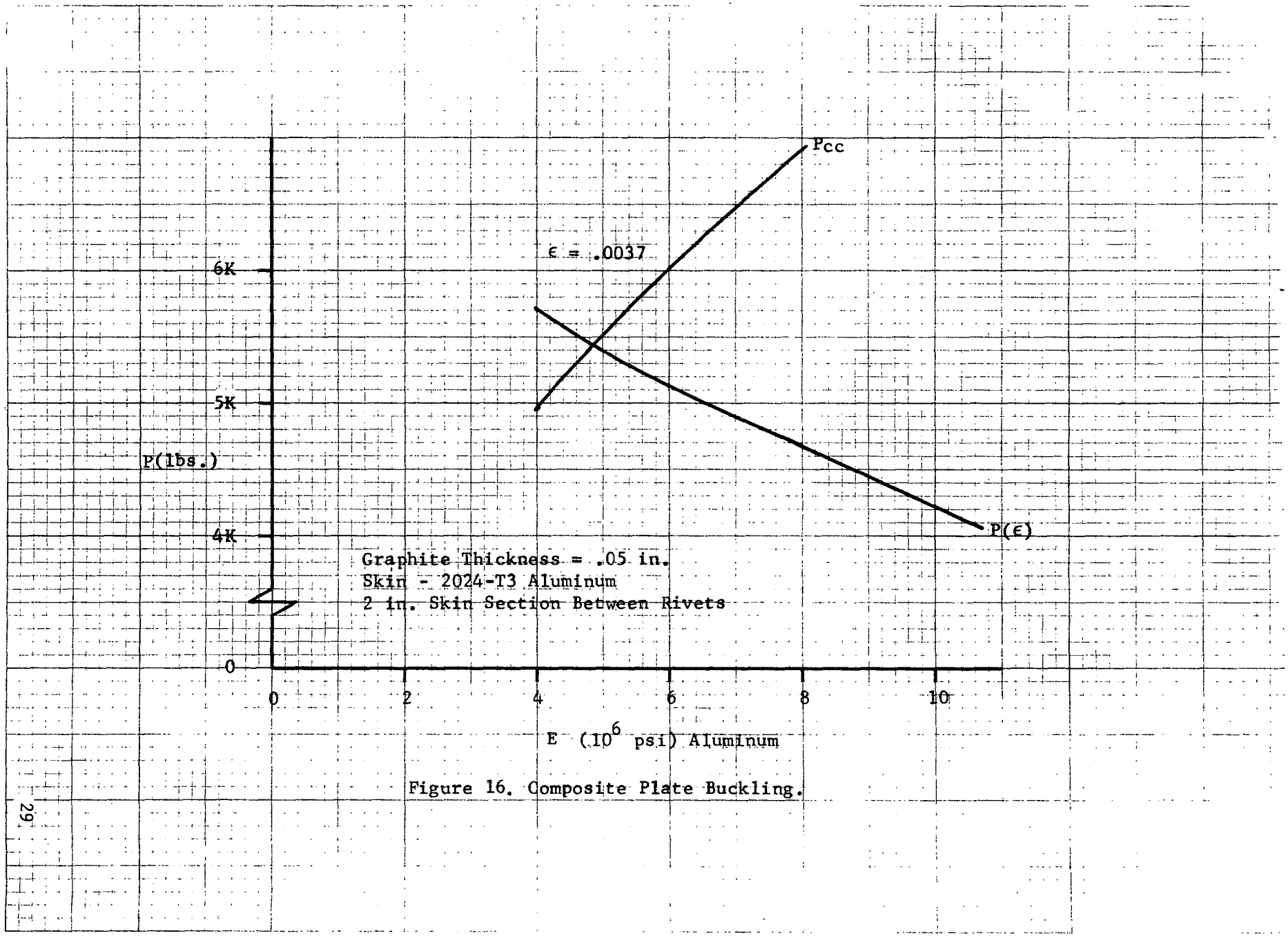

Figure 16. Composite Plate Buckling.

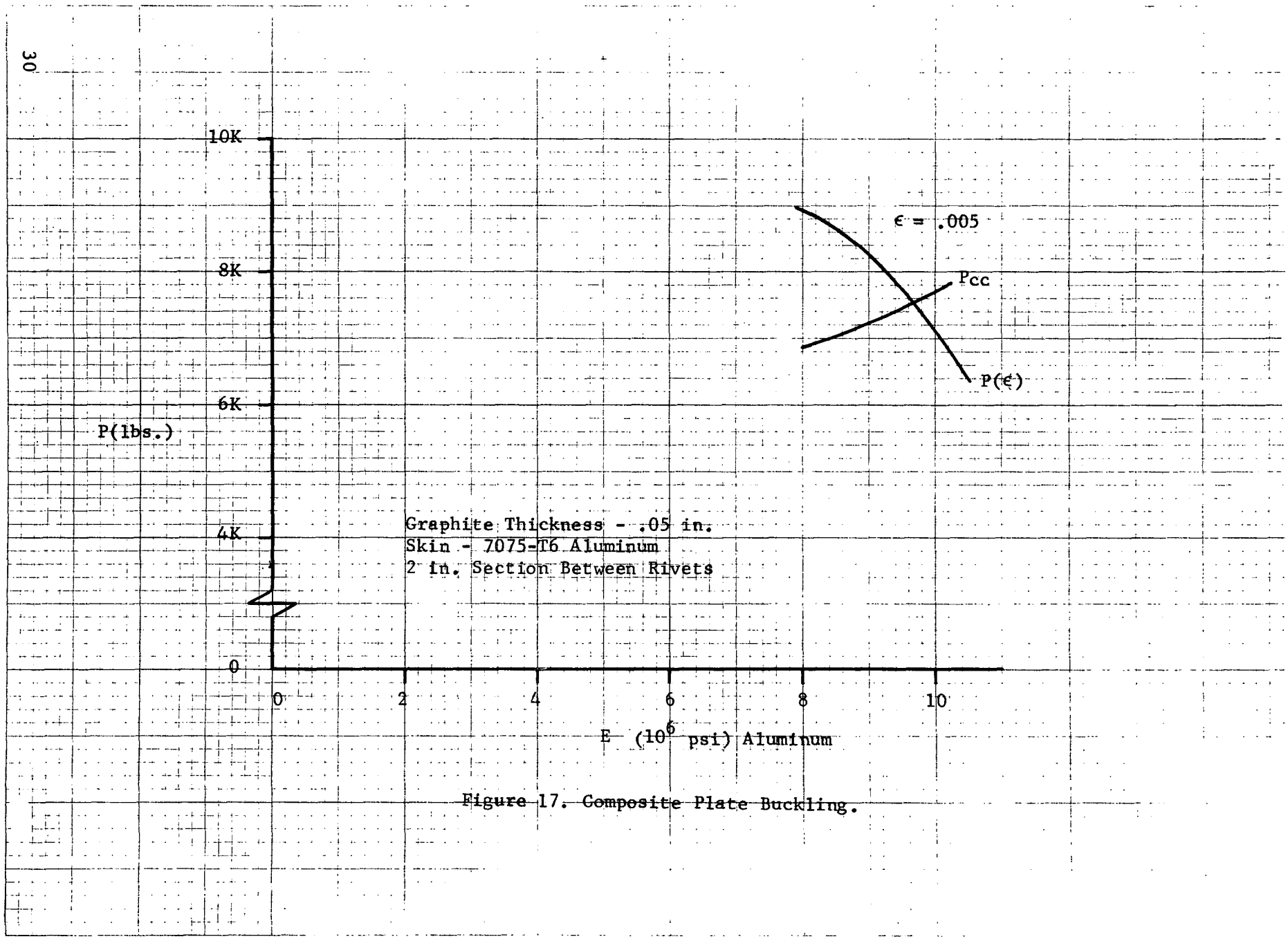

Figure 17. Composite Plate Buckling.

Naturally this imposes a limitation on the width of the graphite strip. The width of the graphite strip was set at one inch. It was deemed desirable to maintain the same thickness of graphite for both the skin and the crown. Since it was recognized that the crown would be considerably more resistant to buckling than the skin, a graphite width of .5 inches was selected.

For the purposes of the optimization analysis the thickness of the graphite was arbitrarily set at .030 in. The graphite selected for calculation was Modmor II. With these considerations in mind an optimization of crown (hat) width and hat height could be made. The only elements to be affected by the variation in parameters were the hat height and crown width. The results of the optimization are plotted in Figure 18.

The results of the optimization indicate that a crown width of .75 inches is most desirable. Any lesser width would conflict with the bonding on of graphite strips since an entirely flat surface is necessary and the bending radius will induce some fringe irregularities. A lower limit of .5 inches was set on the hat height based on fabrication considerations. The optimization presented in Figure 18 was carried out for the 20 in. panel. Although the original desire was for the 20 in. panels to fail in column buckling, the lower limits on the dimensions and the load carrying requirements ruled out such a design. Thus the final dimensions of the aluminum sections have been set. Refer to Figure 22 for the final design. Rivet spacing was set at .5 inches to avoid inter-rivet buckling.

The remaining consideration is graphite thickness. Two approaches may be used to determine this thickness. The first approach determines the thickness based on the loads of the preceding analysis. The second approach determines the thickness based on the preceding analysis with the addition of a thermal preload in the graphite.

As a result of bonding at elevated temperature and subsequently cooling, the graphite will be in compression and the aluminum in tension. Consequently, when the composite strip is loaded in axial compression the graphite will be forced to bear an additional compressive stress to bring the aluminum stress to zero. This stress is

$$\sigma' = \frac{E_1}{E_2} \cdot \frac{(\alpha_1 - \alpha_2) \cdot \Delta T \cdot t_1 \cdot E_1 \cdot E_2}{E_1 \cdot t_1 + E_2 \cdot t_2} \qquad (18)$$

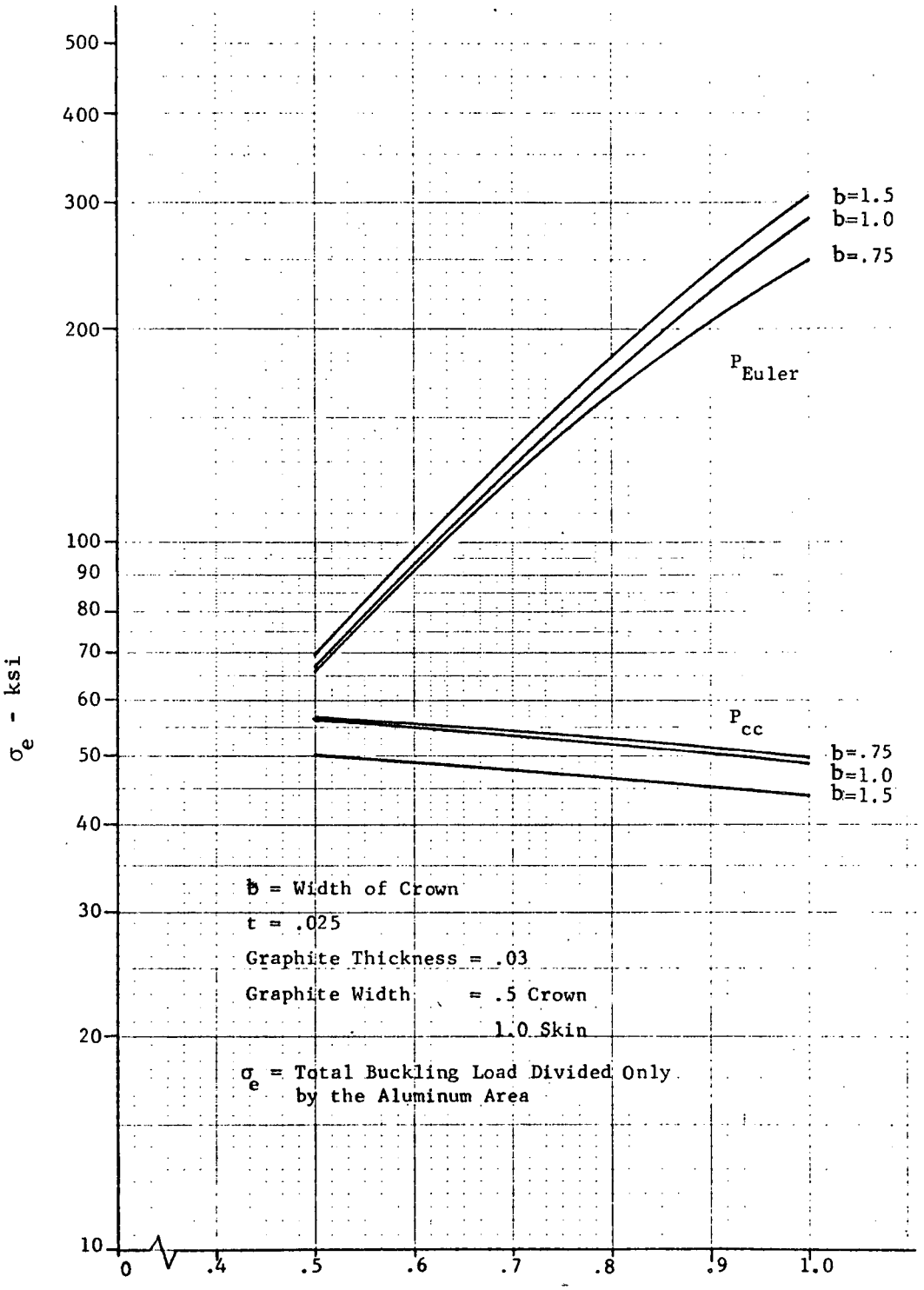

Figure 18. Hat Optimization.

where

t_1 = Thickness of the graphite

t_2 = Thickness of the aluminum

E_1 = Young's modulus of the graphite = 20×10^6 psi

E_2 = Young's modulus of the aluminum = 10.5×10^6 psi

α_1 = Thermal coefficient of expansion of graphite = $-.4 \times 10^{-6} \frac{in}{in\text{-}F^\circ}$

α_2 = Thermal coefficient of expansion of aluminum = $12 \times 10^{-6} \frac{in}{in\text{-}F^\circ}$

Thus, in order to reduce the stress in the aluminum to zero the graphite will bear

$$\sigma_1 = -\frac{E_1}{E_2} \cdot \frac{(\alpha_1-\alpha_2)\cdot\Delta T\cdot t_1\cdot E_1\cdot E_2}{E_1\cdot t_1 + E_2\cdot t_2} - \frac{(\alpha_1-\alpha_2)\cdot\Delta T\cdot t_2\cdot E_1\cdot E_2}{E_1\cdot t_1 + E_2\cdot t_2} \qquad (19)$$

$$= -(\alpha_1-\alpha_2)\cdot\Delta T\cdot E_1 \qquad (20)$$

The additional graphite load resulting from this stress must be added to the total compressive buckling load of the graphite-aluminum plate. At room temperature (65°F), ΔT from the cure temperature is -160F°. Thus the compressive prestress in the graphite is

$$\sigma_1 = -(-.4-12.0)\times 10^{-6}\times(-160)\cdot(20\times 10^6)$$

$$= -40{,}000 \text{ psi}$$

Table VIII presents the loads with and without thermal preloads as a function of graphite thickness. Failure is assumed to occur at a load only negligibly higher than the load at which the first buckle is initiated.

TABLE VIII. – PANEL CRIPPLING LOADS FOR VARYING GRAPHITE THICKNESS

t Graphite in.	2024-T3 Aluminum Load lbs.	Modmor II Graphite Load lbs.	Thermal Graphite Preload +65°F lbs.	Total Load Without Preload lbs.	% Load Carried by Graphite	Total Load With Thermal Preload (65°F) lbs.	% Load Carried by Graphite (65°F)
.01*	6,600	1,320	2,400	7,920	17	10,320	36
.025	12,400	6,320	6,000	18,720	34	24,720	50
.03	12,400	7,600	7,200	20,000	38	27,200	54
.035	12,400	8,880	8,400	21,280	42	29,680	58
.04	12,400	10,120	9,600	22,520	45	32,120	61
.045	12,400	11,400	10,800	23,800	48	34,600	64
.05	12,400	12,680	12,000	25,080	51	37,080	67
.055	12,400	13,920	13,200	26,320	53	39,520	69

*For graphite of this thickness the skin panel will buckle first at a compressive strain of .0011 after the thermal load in the aluminum has been reduced to zero

Based on the analysis conducted by WRD the first buckle will occur in the web (elements 1-2 and 3-4) at a strain of .00211 after the aluminum tensile load from thermal stresses has been reduced to zero. This corresponds to a stress of 22,600 psi for the 2024-T3 aluminum and 42,200 psi for the Modmor II graphite. In addition to the load resulting from this compressive strain, an additional thermal load must be added to the total figure. The thermal load is the load carried by the graphite when the tensile load in the aluminum has been mechanically reduced to zero. If the effect of thermal stresses is neglected it can be seen from Table VIII that a thickness of about .025 will satisfy the 1/3 load carrying requirement and a thickness of from .040 to .050 will satisfy the 1/2 load carrying requirement for the 2024-T3 aluminum-Modmor II combination. Figure 19 plots percentage of load carried by the graphite versus graphite thickness for the case where thermal preloads are included. As can be seen from the graph, a thickness of about .010 will satisfy the 1/3 load carrying requirement and a thickness of about .025 will satisfy the 1/2 load carrying requirement for the same materials combination. Since the first buckle occurs well within the linear elastic range of both the 7075-T6 and the 2024-T3 aluminum alloys, the design thicknesses apply to both materials combinations.

It should be noted, however, that based on preliminary analysis, thicknesses of .032 and .05 were selected to satisfy the 1/3 and 1/2 load carrying requirements for the 7075-T6 aluminum and Modmor II combination. However, based on the analysis presented above, a thickness of .05 for the 1/2 load carrying requirement is still quite satisfactory.

Meeting the load requirement in tension with the same design presents another problem since thermal prestresses produce a significantly different effect.

For tension loading, it is assumed that if all problems of adhesion are solved, failure will occur when the graphite fails. Assuming that the strip is restrained from bowing, the graphite will bear a compressive prestress equal to

$$\sigma_1 = - \frac{\left(\alpha_1 - \alpha_2\right) \cdot \Delta T \cdot E_1 \cdot E_2 \cdot t_2}{E_1 \cdot t_1 + E_2 \cdot t_2} \tag{21}$$

$$\text{or } \epsilon_1 = - \frac{\left(\alpha_1 - \alpha_2\right) \cdot \Delta T \cdot E_2 \cdot t_2}{E_1 \cdot t_1 + E_2 \cdot t_2} \tag{22}$$

Regardless of the behavior of the aluminum, the compressive strain, ϵ_1, must be overcome in addition to ϵ_{tu} if failure is considered to be the failure of the graphite.

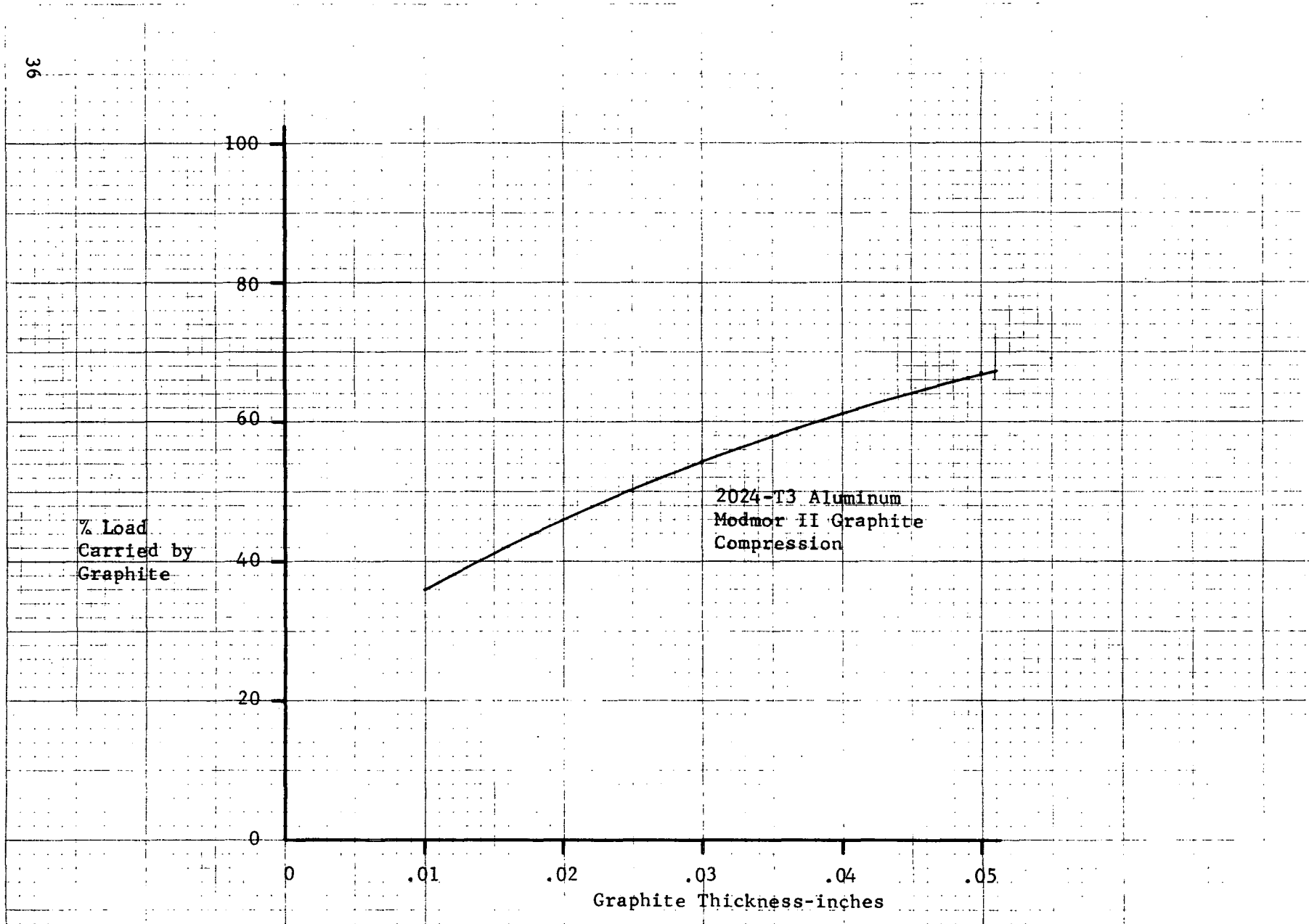

Figure 19. Load Carrying Capacity of Graphite as a Function of Thickness.

Based on the thermal analysis, when the graphite compressive load is reduced to zero the aluminum will be bearing a tensile stress and strain of 21,230 psi and .00198 respectively. From this point the graphite will bear 170,000 psi and a strain of .0085. Thus the strain in the aluminum will be .01048. This corresponds to a stress of roughly 54,000 psi in the 2024-T3 aluminum. Table IX lists total loads and graphite load percentages as a function of graphite thickness. See Figure 20.

TABLE IX. – EFFECT OF GRAPHITE THICKNESS ON PANEL LOADS IN TENSION

Modmor II Graphite t in.	2024-T3 Aluminum Load lbs.	Modmor II Graphite Load* lbs.	Total lbs.	Graphite Load %
.01	29,700	10,200	39,900	26
.02	29,700	20,400	50,100	41
.025	29,700	25,520	55,220	46
.03	29,700	30,600	60,300	57
.035	29,700	35,720	65,420	55
.04	29,700	40,800	70,500	58
.045	29,700	45,920	75,620	61
.05	29,700	51,000	80,700	63

*Note: Loads are roughly the same with and without thermal effects for the 2024-T3 aluminum model due to plasticity.

In addition to the different thicknesses required for tension loading, it should be noted that failure occurs in the plastic range of the aluminum. Thus, different thicknesses would also be required for the 7075-T6 aluminum model. It was decided, therefore, to use the thicknesses determined by the compression analysis rather than present different designs for every loading case.

Based on the predetermined thicknesses for 2024-T3 and 7075-T6 the following buckling loads were calculated (see Table X). Figure 21 presents a plot of weight efficiencies of the reinforced panels with thermal effects included.

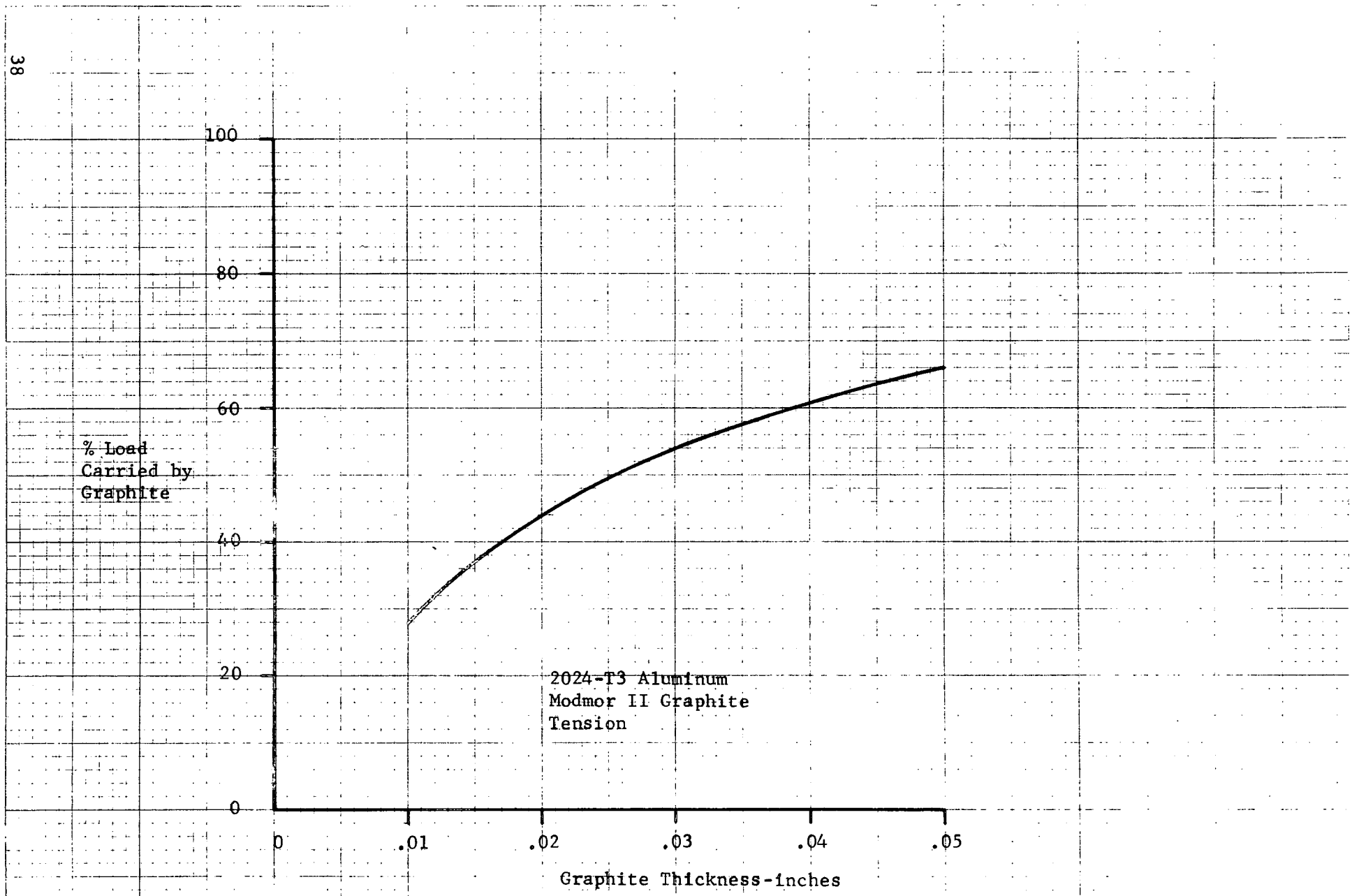

Figure 20. Load Carrying Capacity of Graphite as a Function of Thickness.

TABLE X. — COMPRESSION DESIGN LOADS

Aluminum	Modmor II Graphite Thickness in.	Aluminum Load (lbs)	Modmor II Load (lbs)	Graphite Thermal Preload +65°F(lbs)	Total Load without Preload (lbs)	% Load Carried by Graphite	Total Load with Thermal Preload (lbs)	% Load Carried by Graphite
2024-T3 Designed for 1/3 Load Carried by Graphite	.025	12,400	6,330	6,000	18,730	34	24,720	49
Designed for 1/2 Load Carried by Graphite	.04	12,400	10,130	9,600	22,530	45	32,120	61
7075-T6 Designed for 1/3 Load Carried by Graphite	.032	12,200	8,100	7,680	20,300	40	28,000	56
Designed for 1/2 Load Carried by Graphite	.050	12,200	12,660	12,000	24,860	51	36,860	66

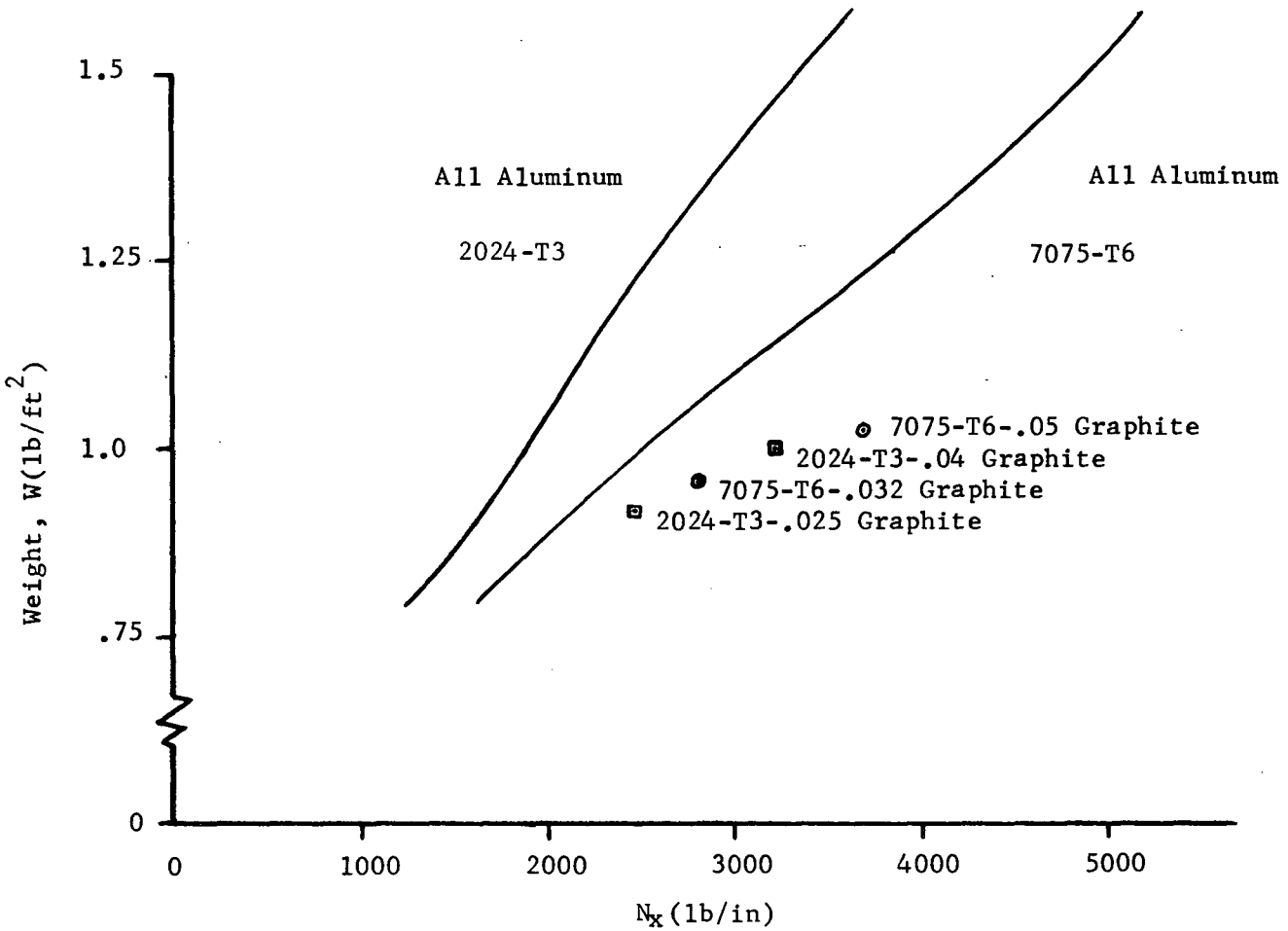

Figure 21. Predicted Weight Efficiencies of Reinforced Panels with Thermal Effects Included.

LOAD TRANSFER ANALYSIS

One of the problems encountered in the design of aluminum-graphite components is the difficulty in joining separate components without destroying the integrity of the system. Since graphite sections generally have much less area than the aluminum sections, area loss due to riveting would greatly reduce the efficiency of the system. In addition, owing to the brittle nature of graphite, it is very difficult to make such connections without inducing cracks critical to normal operation. At present the only effective means of joining aluminum and graphite sections is by bonding. Figure 22 presents an idealized joint scheme formulated by WRD. For ease of integration with metal components, the region at the end of the joint must be all metal. This requirement presents serious problems since the aluminum in the joint is in the plastic range at the failure strain of the graphite.

Tensile ultimate for 7075-T6 is 76,000 psi. If the skin is .025 in. thickness and one inch in width it will bear a load of 1,900 lbs. The skin will transfer most of this load to the graphite in a proportion given by

$$P_1 = \frac{E_1 t_1}{E_1 t_1 + E_2 t_2} \cdot P_2 \qquad (23)$$

Substitution of the appropriate dimensions and properties for Modmor-II graphite and 7075-T6 aluminum results in

$$P_1 = \frac{P_2}{1.26} = 1508 \text{ lbs}$$

If the tensile ultimate of the graphite is set at 170,000 psi, then for a thickness of .05 in. and a width of one inch the graphite will bear a load of 8,500 lbs. Subtracting the load transferred by the skin leaves 6,992 lbs to be carried by the cover plate configuration. Thus the total thickness of the cover plate configuration must be at least .092 in. to avoid tensile ultimate failure of the joint.

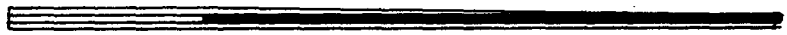

TYPICAL JOINT

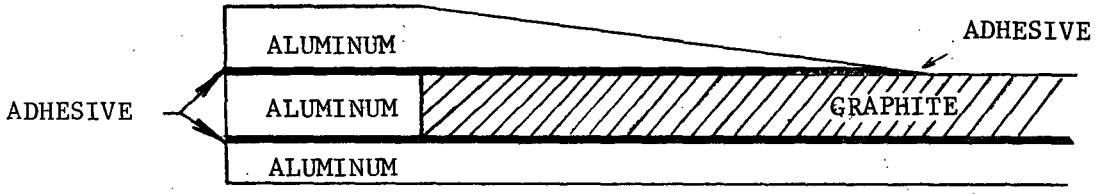

ENLARGED

(NOT TO SCALE)

Figure 22. Idealized Aluminum to Graphite Joint.

The tensile ultimate of 2024-T3 aluminum is 66,000 psi. By the same method as above it was determined that the thickness of the cover plate configuration for the .025 in. 2024-T3 aluminum - .04 in. Modmor II graphite model must be at least .08 in. For the .032 in. Modmor II - .025 in. 7075-T6 model the required thickness is .052 in. For the .025 in. Modmor II - .025 in. 2024-T3 model the required thickness is .046 in.

Thus, to prevent failure across the all aluminum portion of the joint it is recommended that the total thickness of the cover plate configuration be equal to or greater than twice the thickness of the graphite.

High peak shear stresses are also a problem of considerable importance. The ideal approach is to uniformly taper the cover plate configuration from its thickness at the beginning of graphite load transfer to the graphite surface. This scheme is presented in Figure 22. Unfortunately such a cover plate for the thicknesses under consideration is difficult to fabricate without introducing thermal warpage. Thus it was decided to simulate the taper by dividing the thickness of the cover plate configuration among two plates. The length of the lower plate of the configuration was set at 3.5 inches and the length of the upper plate was set at 2.0 inches.

For the .025 in. 7075-T6 aluminum - .05 in. Modmor II graphite model the total load that must be transferred from the cover plate configuration to the graphite is 6,990 lbs. The formulas for the peak values of the shear stress for a single lap shear plate are given by

$$\tau(0) \simeq \frac{G_a}{k \cdot t_a} \cdot \frac{P}{E_2 t_2} \tag{24}$$

$$\tau(L) \simeq \frac{G_a}{k \cdot t_a} \cdot \frac{P}{E_1 t_1} \tag{25}$$

where $\tau(0)$ is the peak shear stress immediately over the beginning of the graphite and $\tau(L)$ is the peak shear stress at the end of the plate and

$$k^2 = \frac{G_a}{t_a}\left(\frac{1}{E_1 t_1} + \frac{1}{E_2 t_2}\right) \tag{26}$$

The cover plate design calls for two plates, the upper plate of which is stepped back 1.5 inches from the lower. Since $\tau(L)$ is divided among two different regions it is not nearly as important as $\tau(0)$.

The exact solution for the peak shear stress distribution through the two plates is difficult and beyond the scope of the present program. It is known however that the P in equation (13) for $\tau(0)$ must lie between 3,495 lbs and 6,990 lbs. This corresponds to an elastic shear strain of from .159 in/in to .317 in/in. Although shear stress-strain curves for Metlbond 225 are not currently available, shear stress-strain curves for other typical structural adhesives such as Metlbond 227, Metlbond 329, and Metlbond 328 indicate that a failure strain of from .1 in/in to .2 in/in is not at all unreasonable. Since the calculated shear strains are based on elastic considerations it is felt that the stress averaging effect of plasticity at these strains will give a more than adequate margin of reliability to the joint.

Final Design

Based on the thermal analysis, the optimization program, and the joint load transfer analysis, the final dimensions for the graphite-aluminum panel configurations were determined. Figure 23 is a drawing of the final panel design. Shown on Table XI are the predictions of failure loads based on the final design.

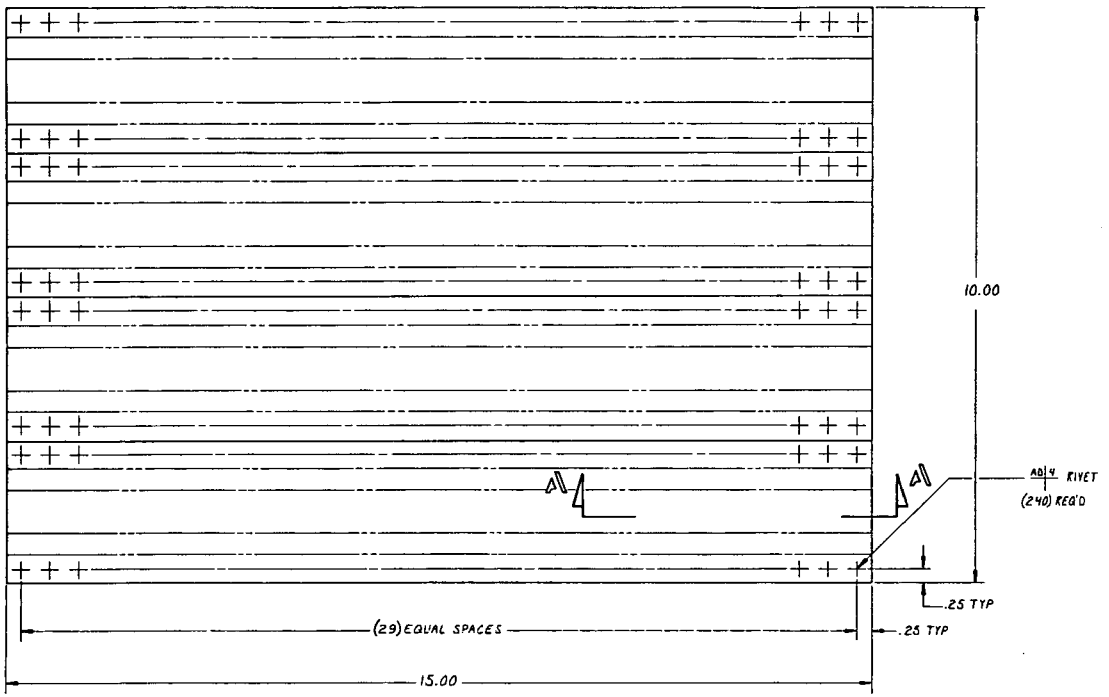

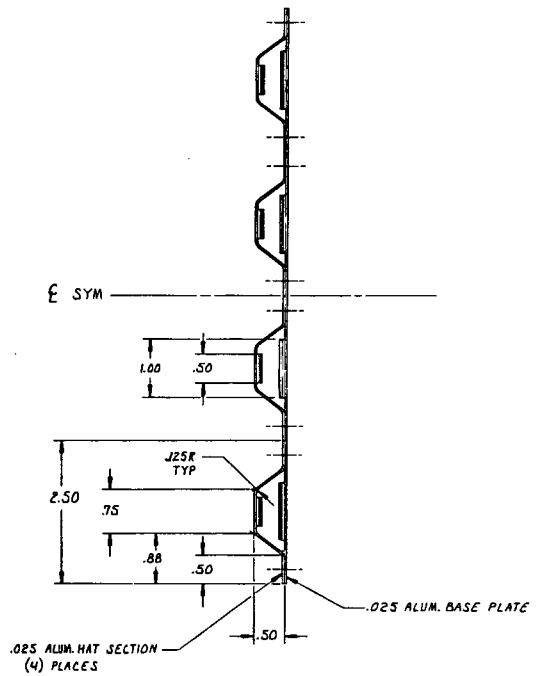

Figure 23. Final Panel Design.

PANEL #	ALUMINUM MATERIAL	GRAPHITE THICKNESS
1	2024-T3	.025
2	2024-T3	.040
3	7075-T6	.032
4	7075-T6	.050

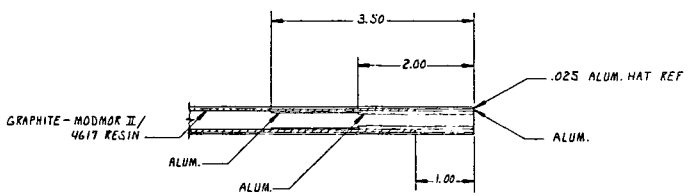

SECTION A-A
ALUM./GRAPHITE JOINT
BOND USING METLSONG 225

QUANTITY REQUIRED	-0	PANEL ASSY
	PART NO.	PART NAME
MANUFACTURING TOLERANCES ARE UNLESS OTHERWISE NOTED: FRACTIONS ± .031; DECIMALS .XX ± .020, .XXX ± .005; ANGLES ±1/2° DEB; ALL MACHINED SURFACES ARE AS NOTED REF. MAS 30	DRAFT	4-29-73
	CHECK	
	DESIGN	
	STRESS	
	PROCESS	
	TOOLING	
	APPROVED	
NEXT ASSEMBLY	NO REQ'D	
CONTRACT NO NAS 1-10507	MJO 4302	

Whittaker RESEARCH & DEVELOPMENT/SAN DIEGO 3540 Aero Court - San Diego, California 92123

PANEL ASSY - GRAPHITE REINFORCED ALUMINUM

SIZE	CODE IDENT NO	DRAWING NO
D	83472	4745

SCALE | CALC | SHEET 1 OF 1

TABLE XI. – FINAL DESIGN LOADS

Design Panel	Compression Load at 1st Buckle Without Thermal Effects lbs.	Compressive Strain in/in	% Load Carried by Graphite Without Thermal Effects	Compression Load at 1st Buckle With Thermal Effects lbs.	% Load Carried by Graphite With Thermal Effects	Tension Load* lbs.	Tension Strain in/in	% Load Carried By Graphite
.025 2024-T3 Aluminum .025 Modmor II Graphite Required Load Carried in Graphite -1/3 Total	18,730	.00211	34	24,720	49	55,220	.0105	46
.025 2024-T3 Aluminum .040 Modmor II Graphite Required Load Carried in Graphite -1/2 Total	22,530	.00211	45	32,120	61	70,500	.0105	58
.025 7075-T6 Aluminum .032 Modmor II Graphite Required Load Carried in Graphite -1/3 Total	20,300	.00211	40	28,000	56	74,440	.0105	44
.025 7075-T6 Aluminum .050 Modmor II Graphite Required Load Carried in Graphite -1/2 Total	24,860	.00211	51	36,860	66	92,800	.0105	55

*Note: Loads Roughly the same with or without Thermal Effects

FABRICATION

The first step in the fabrication procedure was the forming of the hat sections. This was a relatively simple procedure of bending over an edge of given radius. The original specifications called for a bending radius of .010 inches. However, upon inspection of prototype hat sections it was discovered that a bending radius of .010 inches was too severe for the 7075-T6 alloy. There were numerous visible cracks along the bend. Thus, the bending radius was changed to 0.125 for the 7075-T6 hat sections. Although no cracks were then visible it has not been determined how extensive the damage is from microcracks in the bend. Finally, the formed hat sections are placed on a template that sets up the drilling of the rivet holes. The finished aluminum hat sections are presented in Figure 24.

The skin plates were prepared next. A locating template was made to aid the positioning of the riveting template (see Figure 25). The template was set and the holes drilled (Figure 26). Upon completion of the drilling it was necessary to clean the holes of all burrs and debris to prevent possible difficulties in the riveting procedure. This was accomplished by merely going over each rivet hole with a drill bit (see Figure 27).

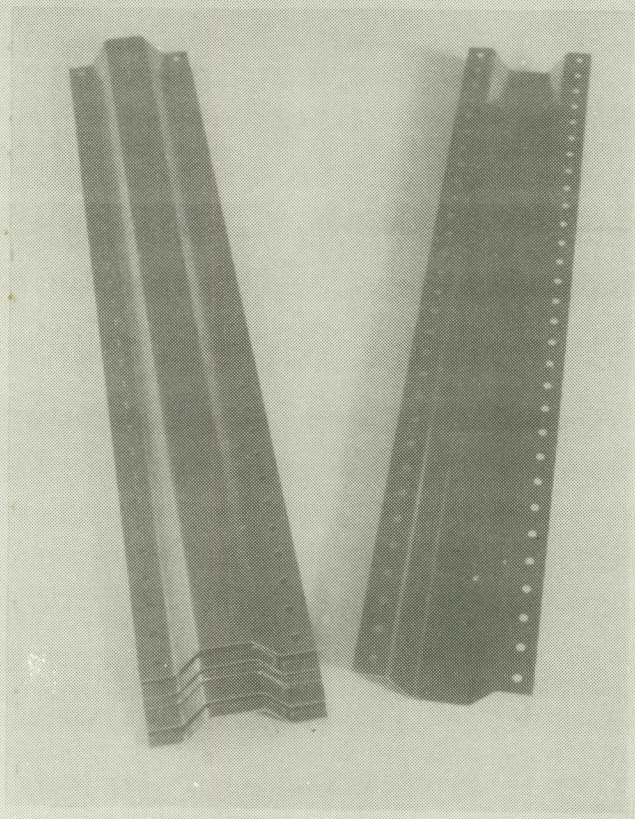

Figure 24. Formed Hat Sections.

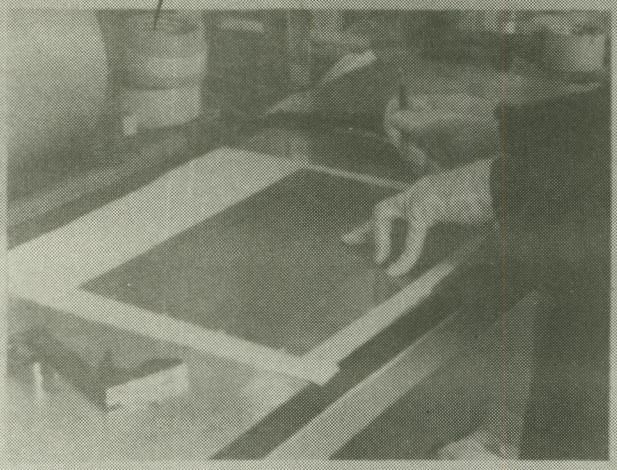

Figure 25. Locating Template.

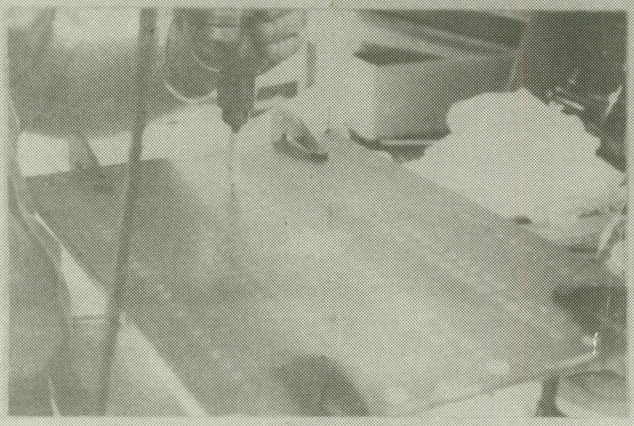

Figure 26. Drilling Template.

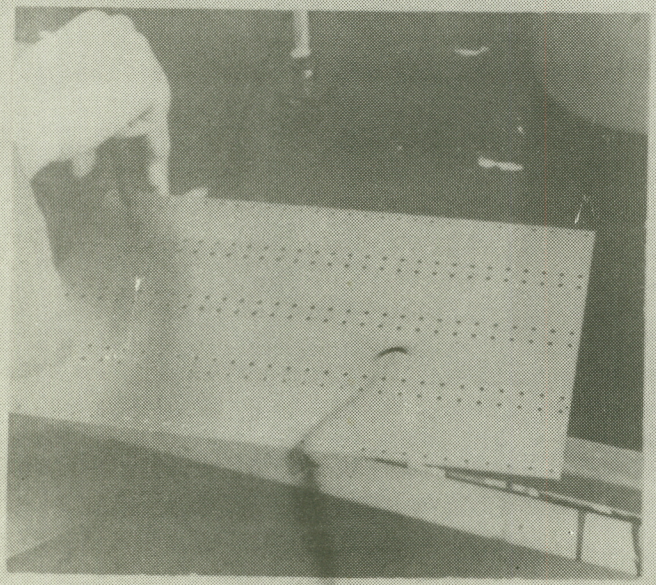

Figure 27. Rivet Hole Finishing.

The next stage of development was the fabrication of the graphite strips. The process was carried out in a number of steps.

STEP I:

The graphite fiber was Modmor II-meter length. It was laid up at 5½ tows/inch.

STEP II:

The fiber layup was impregnated with ERLA/4617 resin giving a resin content of 40 ± 2%.

STEP III:

The prepreg was press laminated into slabs of two different dimensions: 20" x 8½" and 15" x 8" respectively. The different sizes were used to accommodate the already existing panel dimensions. The number of plies used varied with the four thickness requirements. Briefly, they were: .025-3 plies; .032-4 plies; .040-5 plies; .050-6 plies.

STEP IV:

The laminates were cured for 35 minutes at 250°F using contact pressure. After this period 50 psi pressure was applied and the temperature raised to 350°F. The laminates were cured under these conditions for 2 hours. They were then allowed to cool in the ovens to below 150°F before being removed. At the end of the cure the resin content stabilized at 24-30 percent by weight.

STEP V:

The graphite was molded in sheets to the required thickness. The sheets were then cut into strips of the required lengths and widths. The finished laminate strips are presented in Figures 28 and 29.

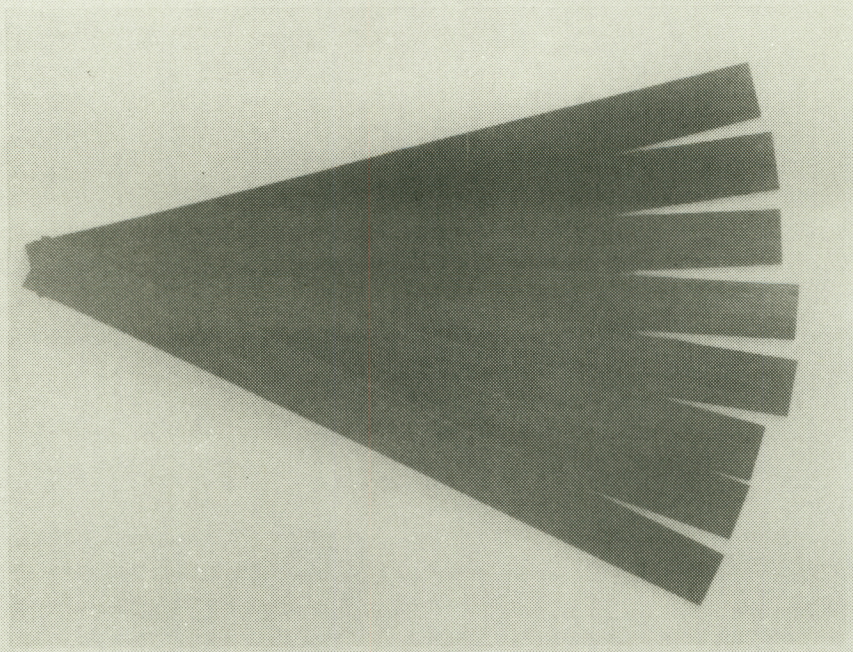

Figure 28. One-Inch Wide Skin Laminates.

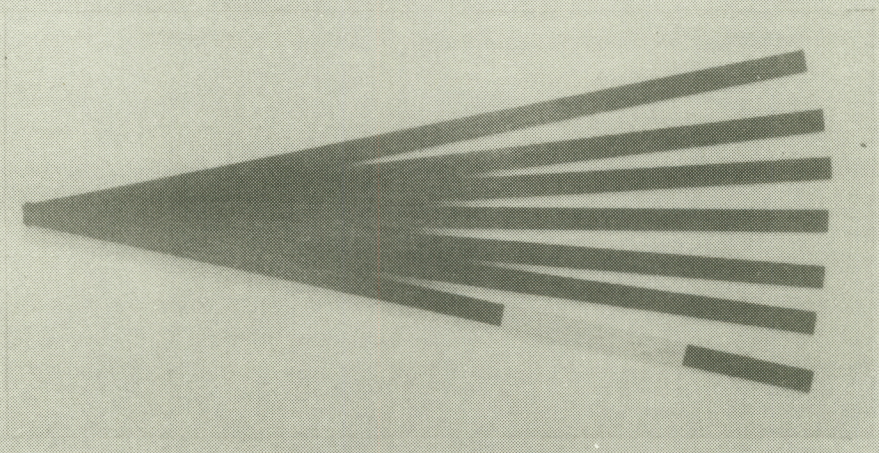

Figure 29. One-Half Inch Wide Crown Laminates.

The next step in the fabrication process was the assembly of the load transfer cover plates and butt plates shown in Figure 30.

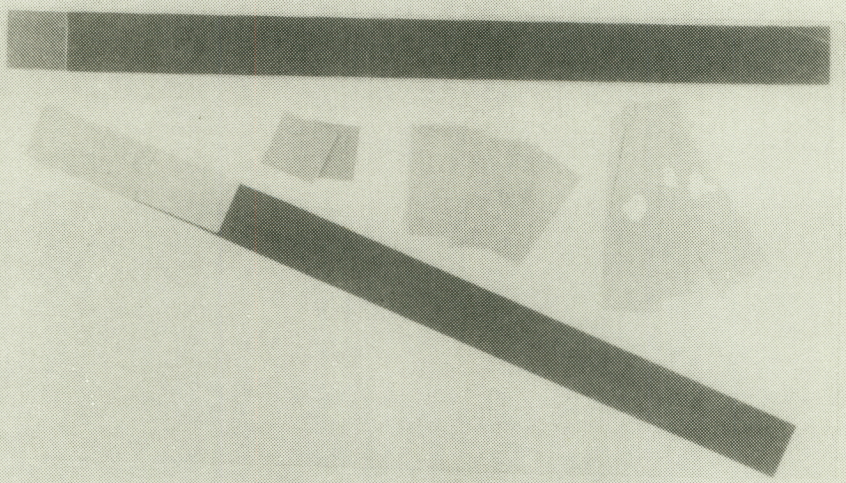

Figure 30. Cover Plates and Butt Plates.

The graphite surfaces were prepared for bonding and laid up on the adhesive film with the butt plate shown in Figure 31. The adhesive film was then cut to size and laid up on the skin and crown sections. The cover plates were then laid up on the graphite strips. The graphite and aluminum sections were then aligned on the plates (see Figure 32). The entire units were then cured at 225°F for 90 minutes at 15 psi. The skins and hats were allowed to cool in the oven to below 150°F. One problem encountered was excess flashing of adhesive. This problem was solved by coating the non-bonding area with a lubricant. After curing, the excess adhesive was mechanically removed.

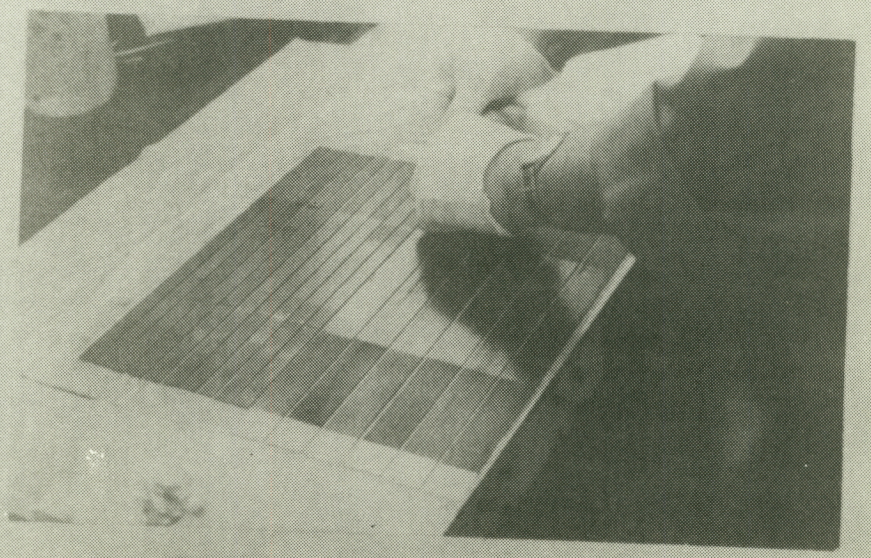

Figure 31. Adhesive-Graphite Layup.

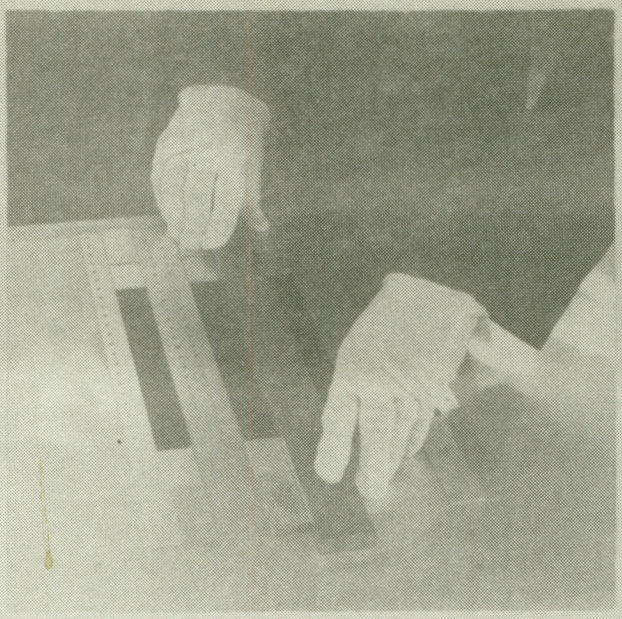

Figure 32. Aligning the Graphite Strips.

The effect of the thermal stresses was immediately apparent (see Figure 33). Owing to the relative position of the aluminum to the graphite, the hat sections were bowed in the same direction as the skin sections. This condition raised the doubt that much of the bowing could be removed.

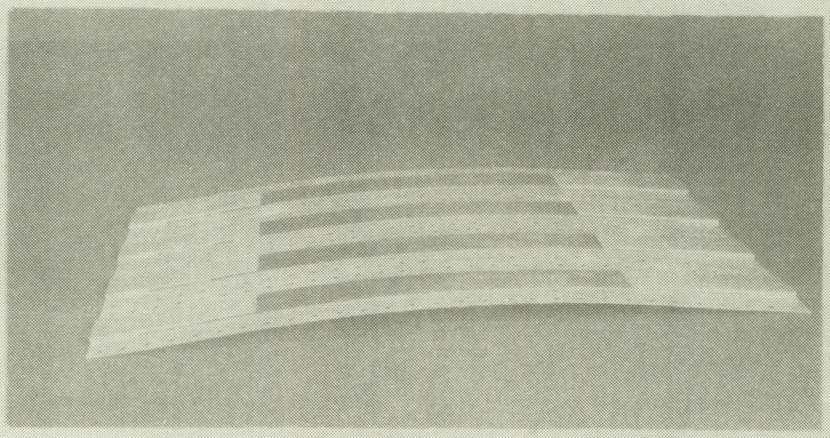

Figure 33. Thermal Bowing.

Fortunately, riveting did remove the major part of the bowing (see Figure 34). The hat sections were then laid up on the skin sections and riveted (see Figures 35 and 36).

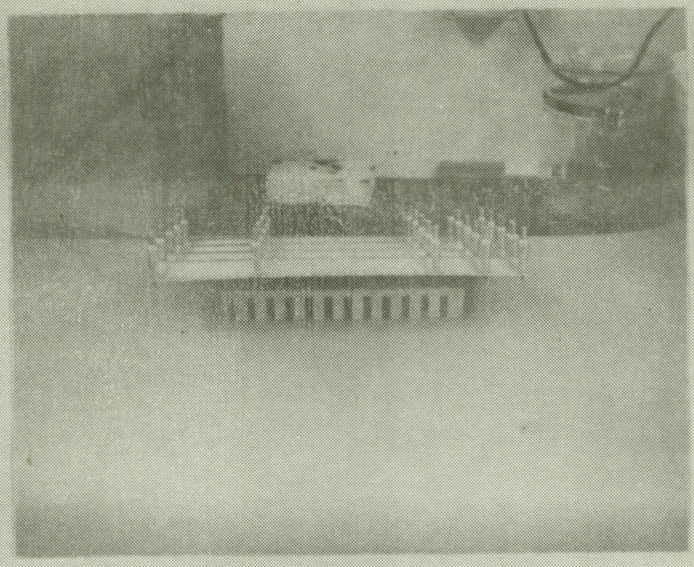

Figure 34. Removal of Bowing with Riveting.

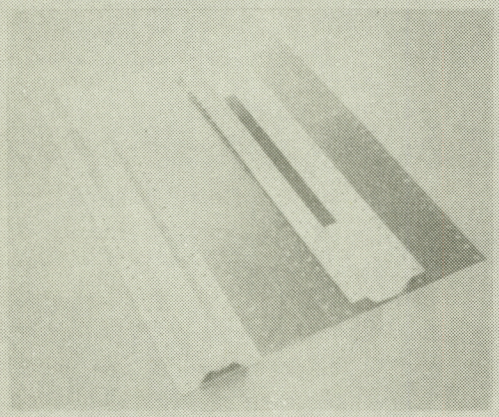

Figure 35. Ready for Riveting.

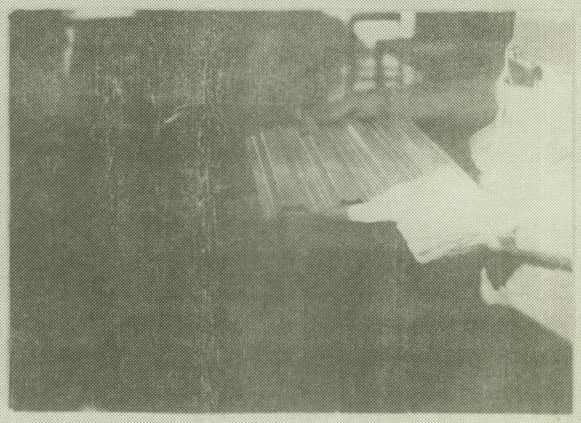

Figure 36. Riveting Procedure.

Early attempts at riveting the panels by hand proved unsatisfactory. Unless proper care was exercised the skin would be transversely strained by the bucking process. This strain is off-set by the spring-like behavior of the hats, which induces a transverse bow (see Figure 37). Thus it was decided to have the panels riveted by a machine that automatically set and expanded the rivets. The resulting panels were much improved. A completed test panel is presented in Figure 38. See Table XII for the proposed testing and thermal cycling schedule.

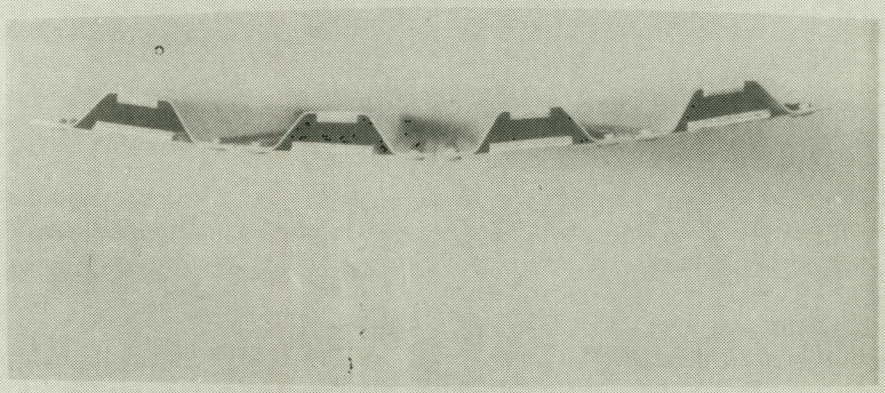

Figure 37. Transverse Bowing.

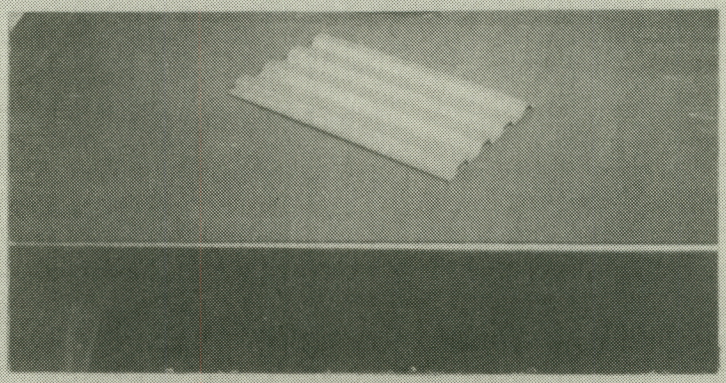

Figure 38. Completed Test Panel.

TABLE XII. — PROPOSED TESTING AND THERMAL CYCLING SCHEDULE

Materials	Panel Identification	Thermally Cycled	Non-Cycled	Tension Test	Compression Test	Shipped To NASA
7075-T6	II-1	x			x	
(.025)	II-2	x			x	
Modmor II	II-3	x			x	
(.05)	II-4		x		x	
10"x15"	II-5		x		x	
	II-6		x		x	
	II-7		x			x
	II-8		x			x
2024-T3	III-1	x		x		
(.025)	III-2	x		x		
Modmor II	III-3	x			x	
(.025)	III-4	x			x	
10"x15"	III-5		x		x	
	III-6		x		x	
	III-7		x			x
2024-T3	IV-1	x		x		
(.025)	IV-2	x		x		
Modmor II	IV-3	x		x		
(.04)	IV-4		x	x		
10"x15"	IV-5		x	x		
	IV-6		x	x		
	IV-7	x			x	
	IV-8	x			x	
	IV-9	x			x	
	IV-10		x		x	
	IV-11		x		x	
	IV-12		x		x	
	IV-13		x			x
10"x20"	IV-14	x			x	
10"x20"	IV-15	x			x	
10"x20"	IV-16	x			x	
10"x20"	IV-17		x			x
2024-T3	V-1	x			x	
(.025)	V-2		x			x
Modmor I (.025)						

THERMAL CYCLING

The test program called for the panels (a representative sampling) to undergo 500 thermal cycles from +160°F to -65°F. The test group at WRD devised a thermal cycling apparatus depicted schematically in Figure 42. The apparatus was basic in concept. Those panels to be cycled would be arranged in a box constructed of heavy-gage aluminum. The box had holes that served not only as vents but held tubes that acted as supports and carriers of electrical heating units (see Figure 39).

The entire unit was placed in a 500°F oven. The unit was placed open face backwards against the back of the oven with all free spaces filled with thermal insulation. This allowed heat transfer to occur primarily through the side vents via a blower. This setup, was an improvement over several other methods tried and resulted in heat up times (-65°F to 160°F) of five to six minutes. All contact points of the box with the oven were insulated (see Figure 40). The oven remained on at all times. The coolant was liquid nitrogen. It was released under pressure at the required intervals and piped into the cycling box. The tube was designed to vent the nitrogen into the box in a fine spray producing an even cooling down phase. At three levels in the cycling box thermal sensors were positioned.

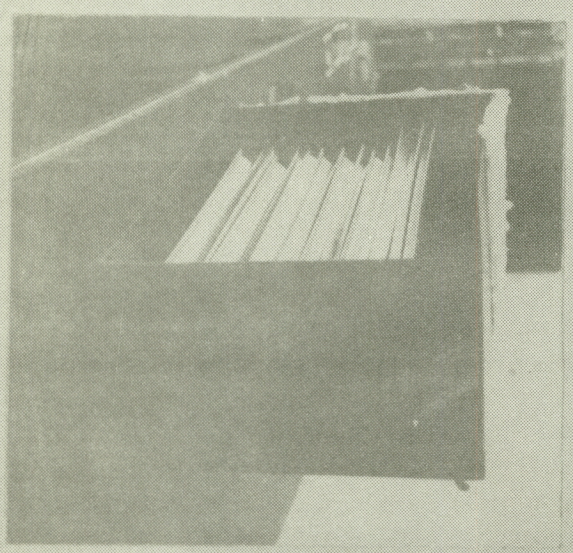

Figure 39. Cycling Box.

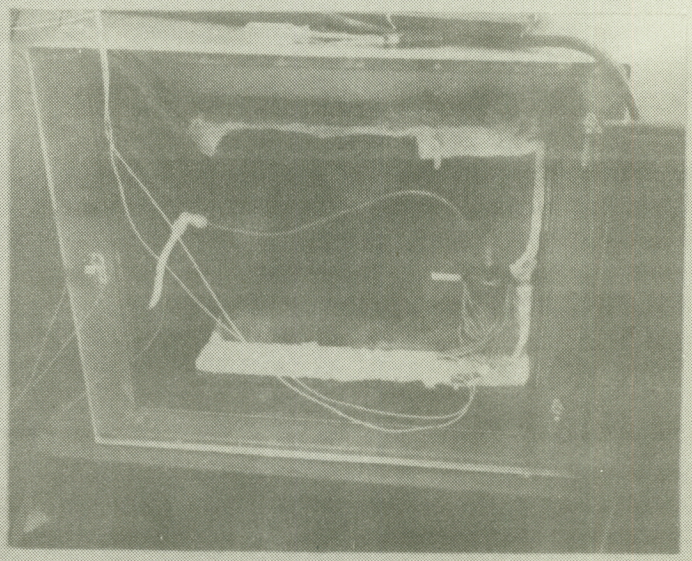

Figure 40. Oven and Cycling Box.

The data from these sensors was fed into a recorder that averaged the temperature readings throughout the box (see Figure 41). The recorder, upon receiving data for the top temperature, automatically triggered the release of liquid nitrogen. The original system featured an automatic switch from an Instron test recorder. After this switch malfunctioned during one of the runs, two redundant switches were installed to shut the entire system off if a predetermined variance occurred.

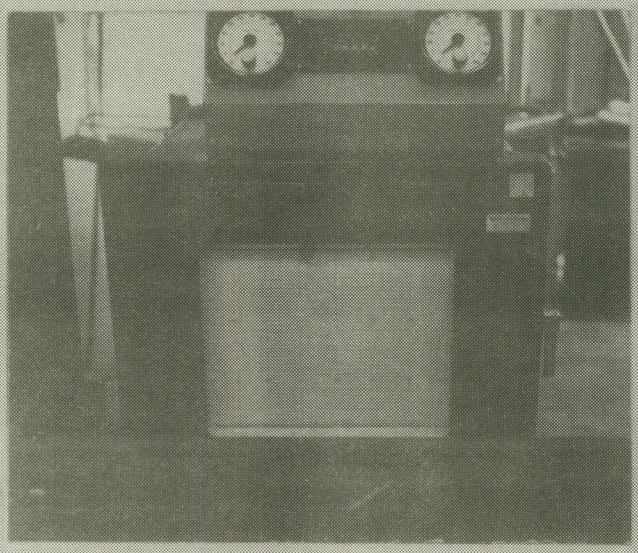

Figure 41. Barber-Colman Recorder.

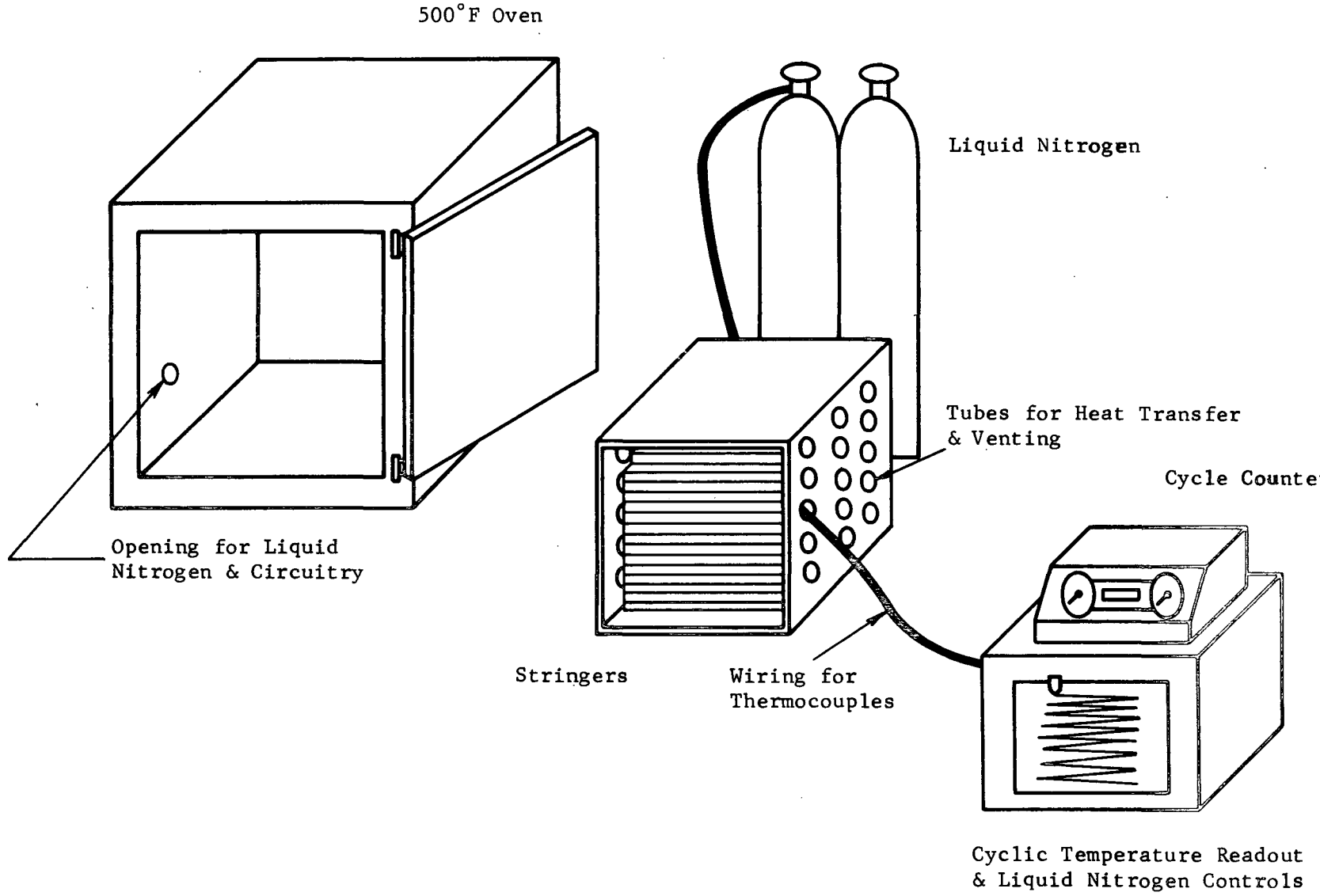

Figure 42. Thermal Cycling Setup.

RESULTS OF THERMAL CYCLING

The results of the thermal cycling are at this time inconclusive. Of the seventeen panels that were cycled six failed or received sufficient damage to rule out further testing. The nature of the failures was graphite debonding. It cannot be ascertained, based on the limited results available at this time, whether this failure was the result of poor bonding or thermal phenomena. Several sections of debonded cover plates had a significant amount of graphite on the adhesive surface. This may have been caused by the flexure occurring during the test. The panel failures tended to group themselves in those specimens with the thicker graphite strips. The following distribution occurred: Modmor II - 2 of 3 .050 thickness graphite panels; 3 of 9 .040 thickness graphite panels; Modmor I - 1 of 1 .025 graphite panel. If indeed the failures were caused by poor bonding it is reasonable to assume that thicker graphite, with its attending higher shear stresses, could have been a contributing factor. In addition, the bulk of the debonding occurred on the skin surfaces, although there were several instances of debonding in the crown. It is also reasonable to assume that since the skin section presents a larger span of material, the graphite-aluminum combination will have larger deformations in this area and that this will at least contribute to the weakening of the bond. Further testing in this area is recommended.

TESTING PROGRAM

Tension Tests

The first step in the testing program was the development of suitable test fixtures. Tension testing was the most difficult case to be considered. Based on the predictions of Table XI and the proposed testing schedule of Table XII, the fixture would have to transfer at least 71,000 lbs to the .025 in. 2024-T3 - .04 in. Modmor II model. In addition it appeared almost impossible to load the panels through the design joints using conventional testing equipment in a manner that would realistically reflect operational loading. In order to load the hat-skin combination uniformly it was decided to resort to shear transfer through a potting compound. The compound selected was Epon 826 - 50% glass bead composition. Thus, attempting to test the joint effectiveness was sacrificed in favor of finding a suitable means of testing the panel, which was the primary goal.

The next problem encountered was finding a suitable means of transferring load through the potting to the panel. The easiest means of achieving this is by bonding on thick steel plates to the potting compound. This method is expensive and time consuming however. Clearly, if a means could be found to grip the entire width of the panel, the problem would be solved. Unfortunately such a method would have necessitated considerable expenditures and modifications of existing test equipment. The use of smaller grips would result in failure between the grips and the potting.

Another method is to fasten steel plates to the potting with bolts. WRD attempted to load the panels in this manner (see Figure 43) but ran into problems with net tension failures.

After failing the panel in net tension an attempt was made to load the panel in the same manner but with only two hat-skin sections (see Figure 44). The problem encountered was net shear failure (see Figure 45). This approach was used again but with the panel necked down to one hat-skin section (one hat-skin section had been previously removed). Again the panel failed in net shear (see Figure 46). This method was found to be effective for the panels utilizing the .025 in. Modmor II graphite (see Figures 47 and 48).

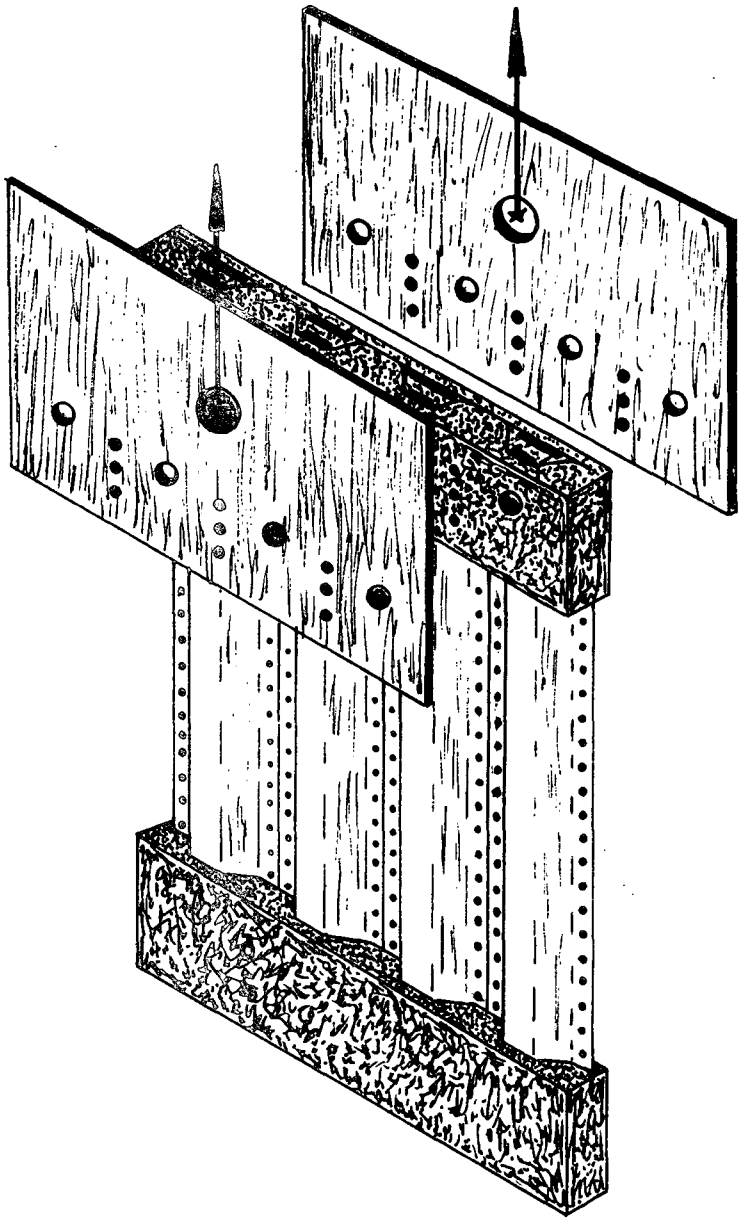

Figure 43. Potting and Tensile Test Fixture.

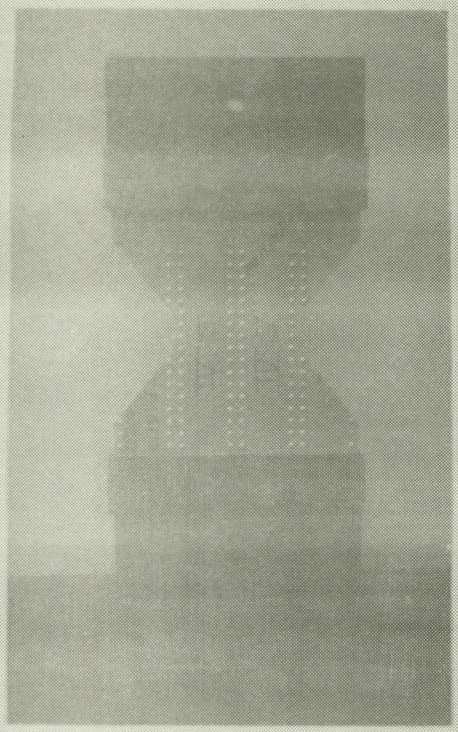

Figure 44. Necked-Down Tension Specimen.

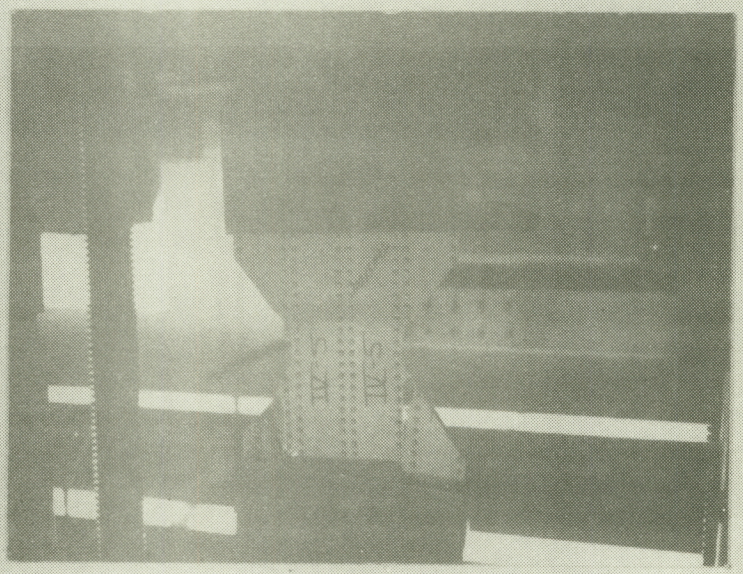

Figure 45. Failed Specimen.

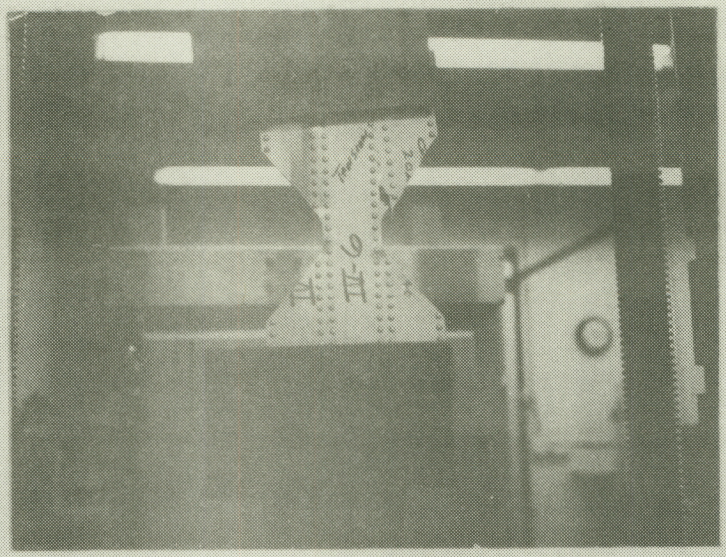

Figure 46. Failed Necked-Down Specimen.

Figure 47. Failed Necked-Down Section.

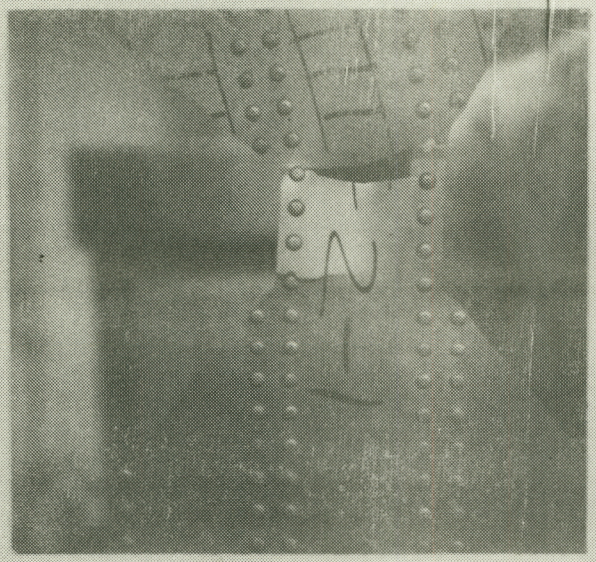

Figure 48. Failed Necked-Down Section.

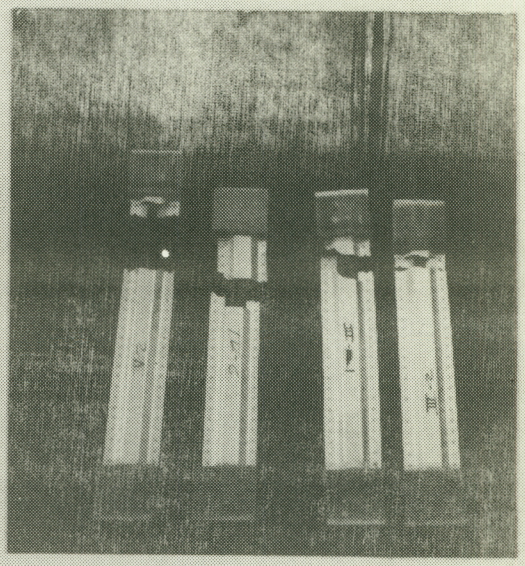

Figure 49. Failed Single Hat Sections.

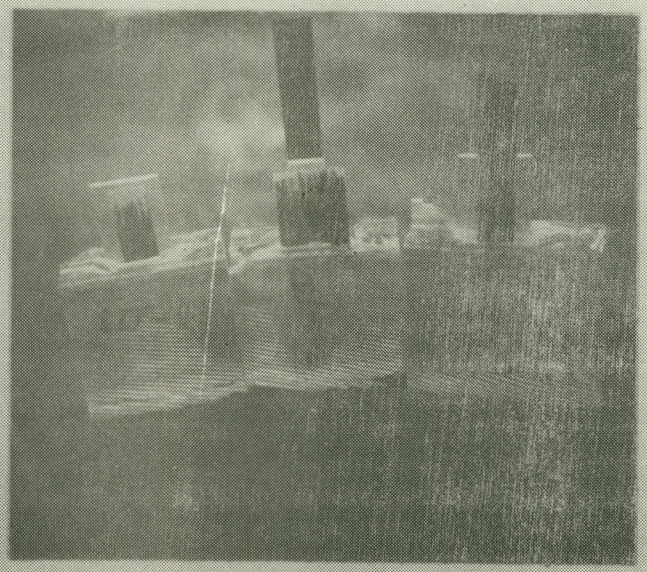

Figure 50. Inspection of Fracture.

The final approach adopted was testing a single hat-skin panel with smaller grips that were suited to the existing test apparatus (see Figures 49 and 50). This proved to be very successful.

A typical load vs. strain plot is presented in Figure 51. The cross-head speed was .050 in/min.

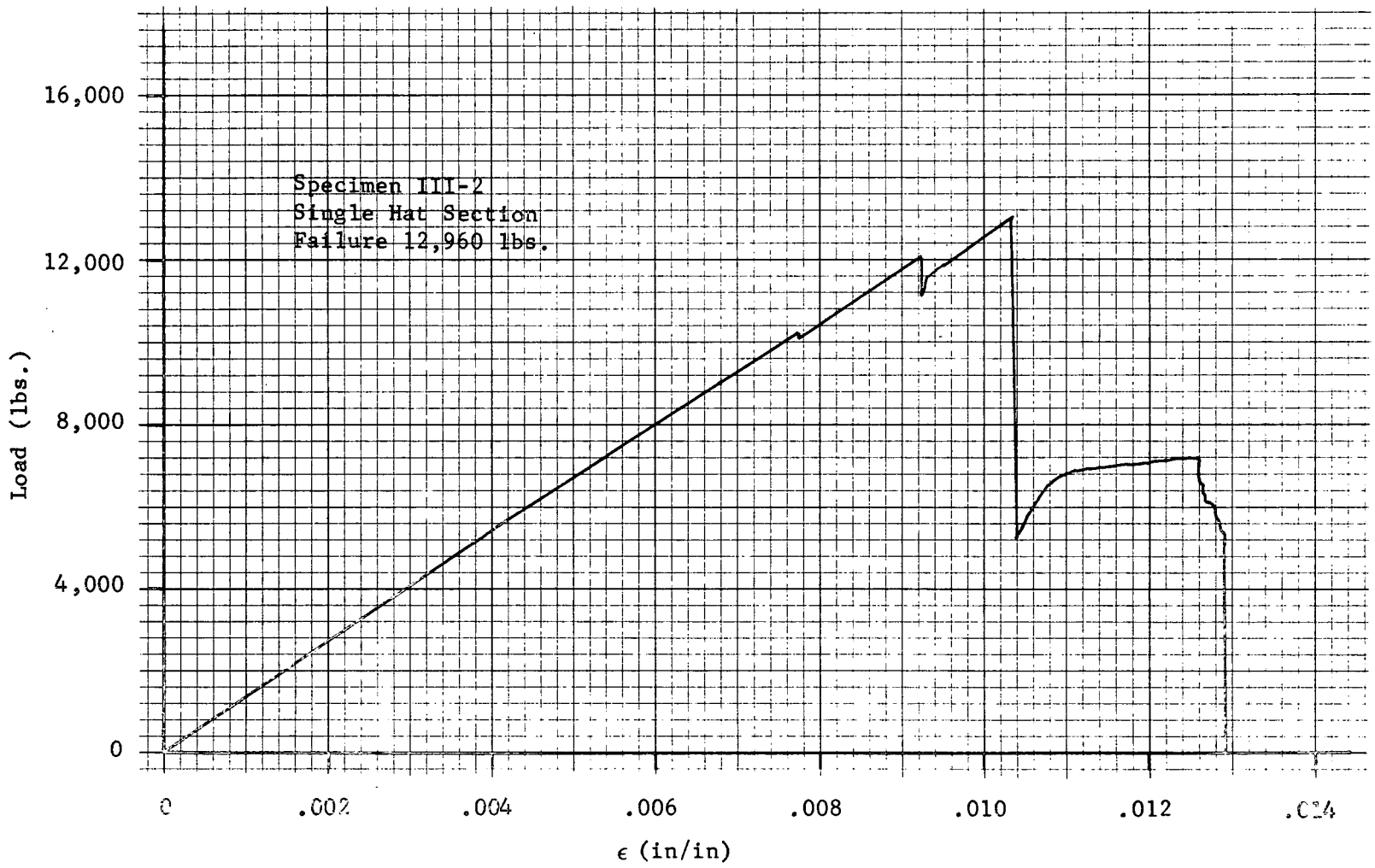

Figure 51. Typical Tension Test.

Compression Tests

The principal concern in the compression test program was the initial bowing of the specimens due to thermal warpage. For the shorter panels the problem was solved by flattening the panels during the potting procedure. The cured potting successfully restrained the initial bowing. However, the potting was not entirely effective in restraining the bowing of the 20 inch panels. Consequently the long panels failed prematurely in column bowing, which precipitated local crippling (see Figure 52).

Figure 53 illustrates the strain gage and LVDT (linear variable differential transformer) placement. The strain gages were placed primarily to attempt to record displacements relating to the mechanics of the local crippling and overall instability. Unfortunately, irregularities in the buckling mode from one panel to another ruled out the formulation of any conclusions. Figures 54 and 55 present the test setup for the compression tests. The top of the potting was machined off to produce a smooth flat surface. Flat steel plates were placed between the specimen and the crosshead and the load cell. This was to insure an even distribution of load. The load cell was a slotted bar of aluminum with strain gages placed inside. It is visible in Figure 55.

Figures 56 and 57 present typical buckling modes for the compression specimens. Generally, failure occurred soon after a buckling mode such as depicted in Figures 56 and 57 appeared. For a complete breakdown of the failure loads refer to Table XIII. Figures 58 and 59 present typical load versus strain plots for the compression specimens.

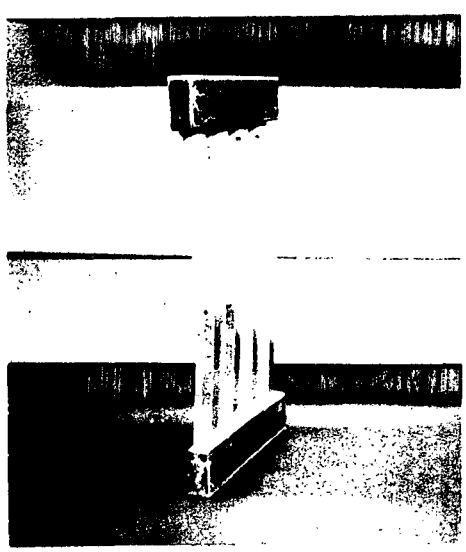

Figure 52. Bowed Long Panel.

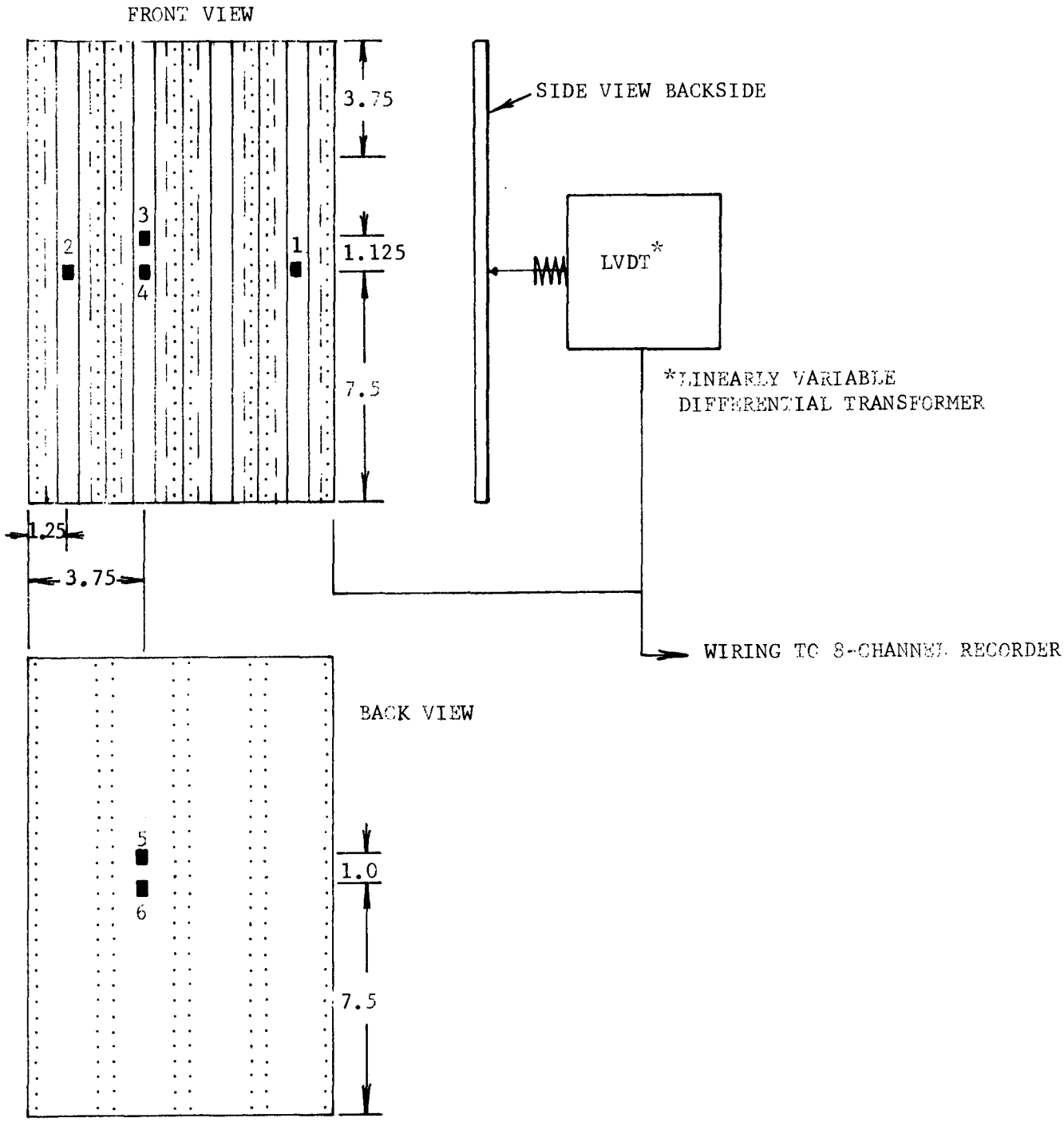

Figure 53. Strain Gage and LVDT Placement.

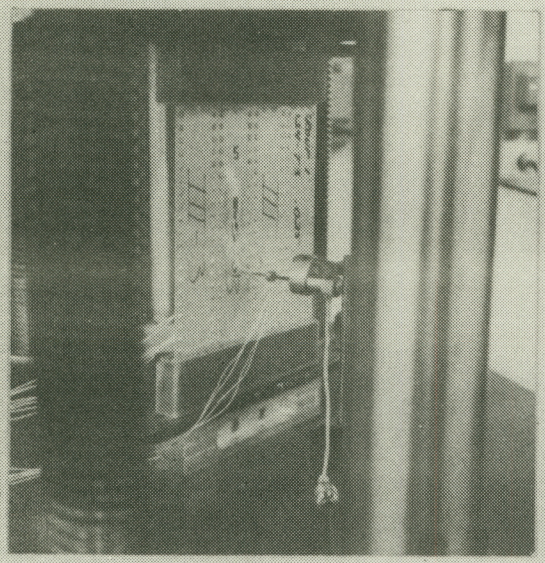

Figure 54. Test Setup.

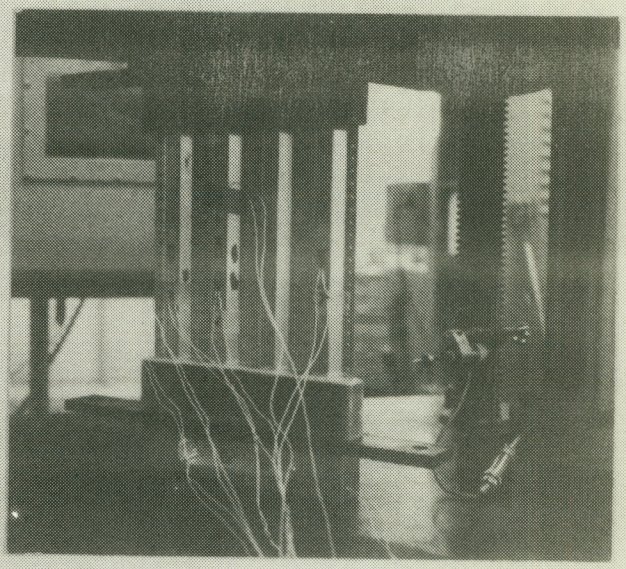

Figure 55. Test Setup.

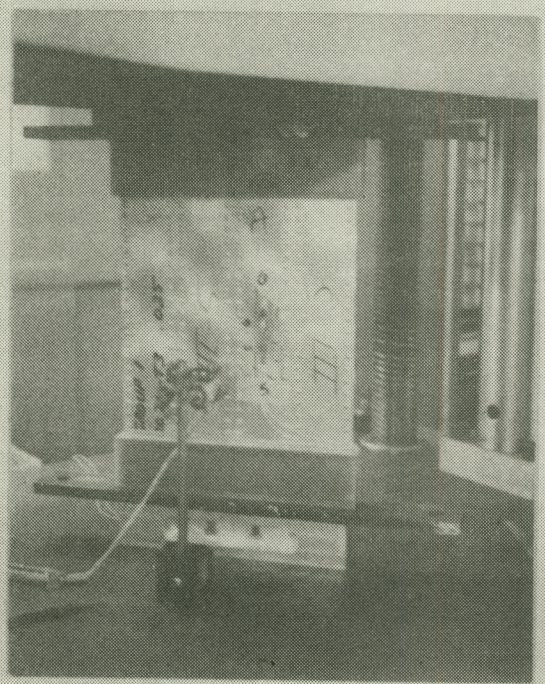

Figure 56. Compression Buckling Mode.

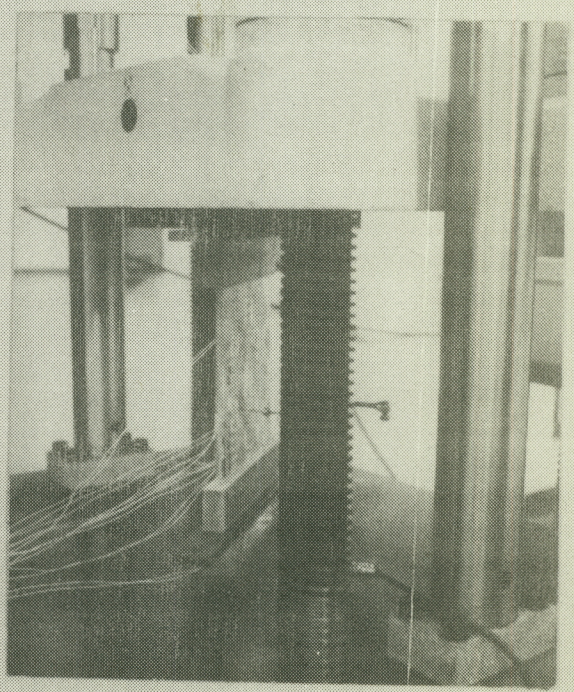

Figure 57. Compression Buckling Mode.

TABLE XIII. — TEST RESULTS

Materials	Panel Identification	Thermally Cycled	Non-Cycled	Tension Test	Compression Test	Failure Load kips				Type of Failure
						Predicted		Test	BUCLASP (4) NASA Prediction	
						(2)	(3)			
.025 Thickness 7075-T6 Aluminum .05 Modmor II Panels 10"x15"	II-1	x			x	-24.9	-36.9			Thermal Cycling
	II-2	x			x	-24.9	-36.9	-25.4	-24.1	Local Buckling
	II-3	x			x	-24.9	-36.9	--	--	Thermal Cycling
	II-4		x		x	-24.9	-36.9	-23.8	-24.1	Local Buckling
	II-5		x		x	-24.9	-36.9	-28.3	-24.1	Local Buckling
	II-6		x		x	-24.9	-36.9	-23.0	-24.1	Local Buckling
.025 Thickness 2024-T3 Aluminum .025 Modmor II Panels 10"x15"	III-1A(1)	x		x		13.0	13.0	11.1	--	Tension
	III-1B	x		x		13.0	13.0	12.7	--	Tension
	III-1C	x		x		13.0	13.0	12.7	--	Tension
	III-1D	x		x		13.0	13.0	11.6	--	Tension
	III-2A	x		x		13.0	13.0	13.7	--	Tension
	III-2B	x		x		13.0	13.0	13.7	--	Tension
	III-3	x			x	-18.7	-24.7	-19.4	- 9.9	Local Buckling
	III-4	x			x	-18.7	-24.7	-19.4	- 9.9	Local Buckling
	III-5		x		x	-18.7	-24.7	-21.4	- 9.9	Local Buckling
	III-6		x		x	-18.7	-24.7	-18.8	- 9.9	Local Buckling

(1) Sequential letters refer to tests of single hats

(2) Prediction without thermal effects

(3) Prediction with thermal effects

(4) Reference two. This program predicts initial buckling only

TABLE XIII. – (Concluded)

Materials	Panel Identification	Thermally Cycled	Non-Cycled	Tension Test	Compression Test	Failure Load kips				Type of Failure
						Predicted		Test	BUCLASP (4) NASA Prediction	
						(2)	(3)			
.025 in. 2024-T3 Aluminum .04 in. Modmor II Graphite Panels 10"x15"	IV-1	x		x		70.5	70.5	--		Thermal Cycling
	IV-2A	x		x		17.6	17.6	13		Debonding & Tension
	IV-2B	x		x		17.6	17.6	13.4		Debonding & Tension
	IV-2C	x		x		17.6	17.6	12.2		Debonding & Tension
	IV-2D	x		x		17.6	17.6	14.7		Debonding & Tension
	IV-3	x		x		70.5	70.5	--		Thermal Cycling
	IV-4		x	x		70.5	70.5	37.8		Net Tension - Joint
	IV-5		x	x		35.3	35.3	24.6		Net Shear - Double Hat Section
	IV-6A		x	x		17.6	17.6	16.7		Net Shear - Single Hat Section
	IV-6B		x	x		17.6	17.6	12.1		Debonding & Tension
	IV-7	x			x	-22.5	-32.1	-23.9	-15.2	Local Buckling
	IV-8	x			x	-22.5	-32.1	-23.6	-15.2	Local Buckling
	IV-9	x			x	-22.5	-32.1	-22.8	-15.2	Local Buckling
	IV-10		x		x	-22.5	-32.1	-23.5	-15.2	Local Buckling
	IV-11		x		x	-22.5	-32.1	-24.1	-15.2	Local Buckling
	IV-12		x		x	-22.5	-32.1	-23.3	-15.2	Local Buckling
Panels 10"x20"	IV-14	x			x	-22.5	-32.1	--	- 9.1	Thermal Cycling
	IV-15	x			x	-22.5	-32.1	-19.3	- 9.1	Column Bowing & Local Crippling
	IV-16	x			x	-22.5	-32.1	-15.1	- 9.1	Column Bowing & Local Crippling
.025 in. 2024-T3 .025 in. Modmor I	V-1	x			x	--	--	--	--	Thermal Cycling

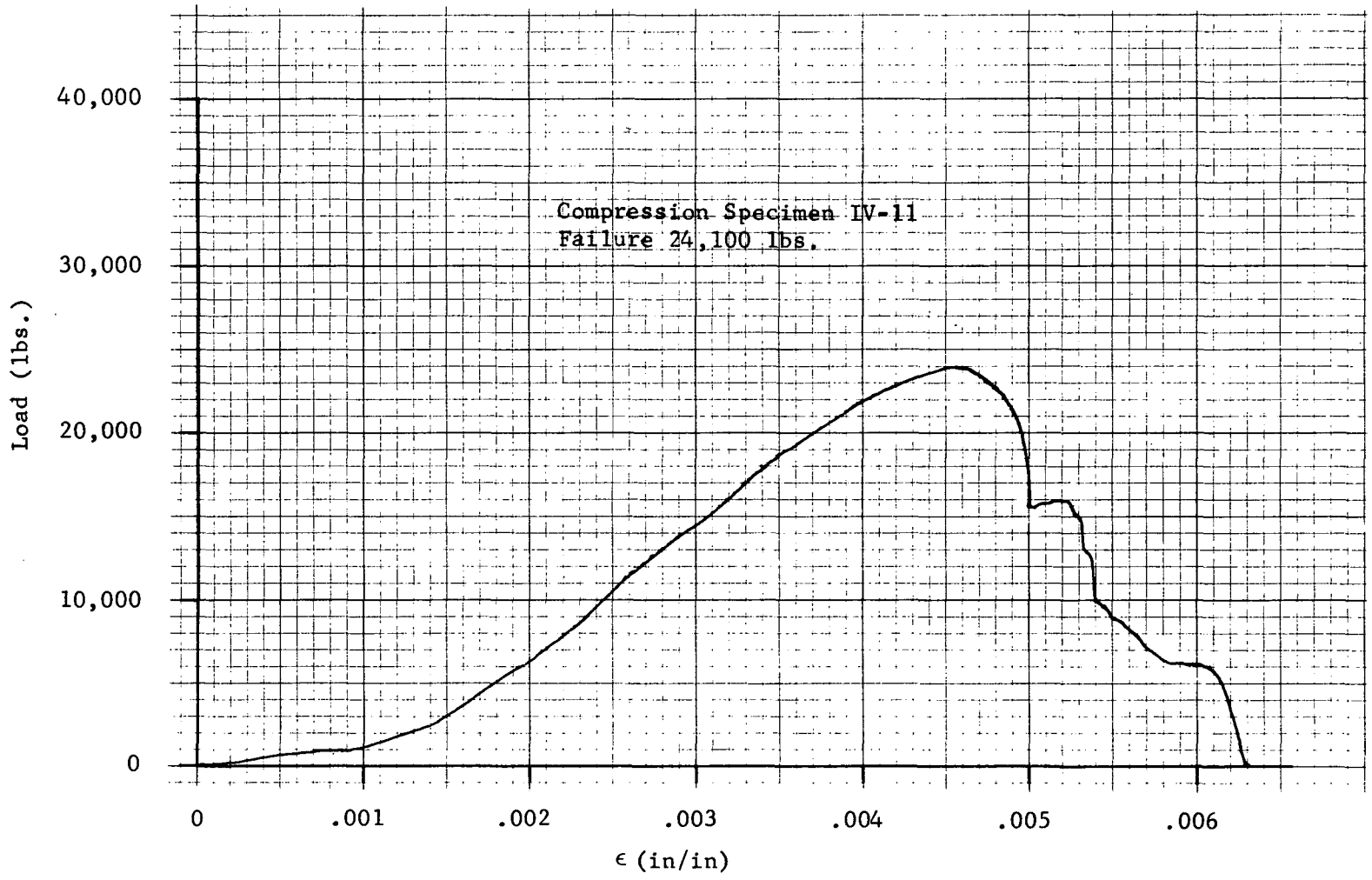

Figure 58. Typical Compression Test.

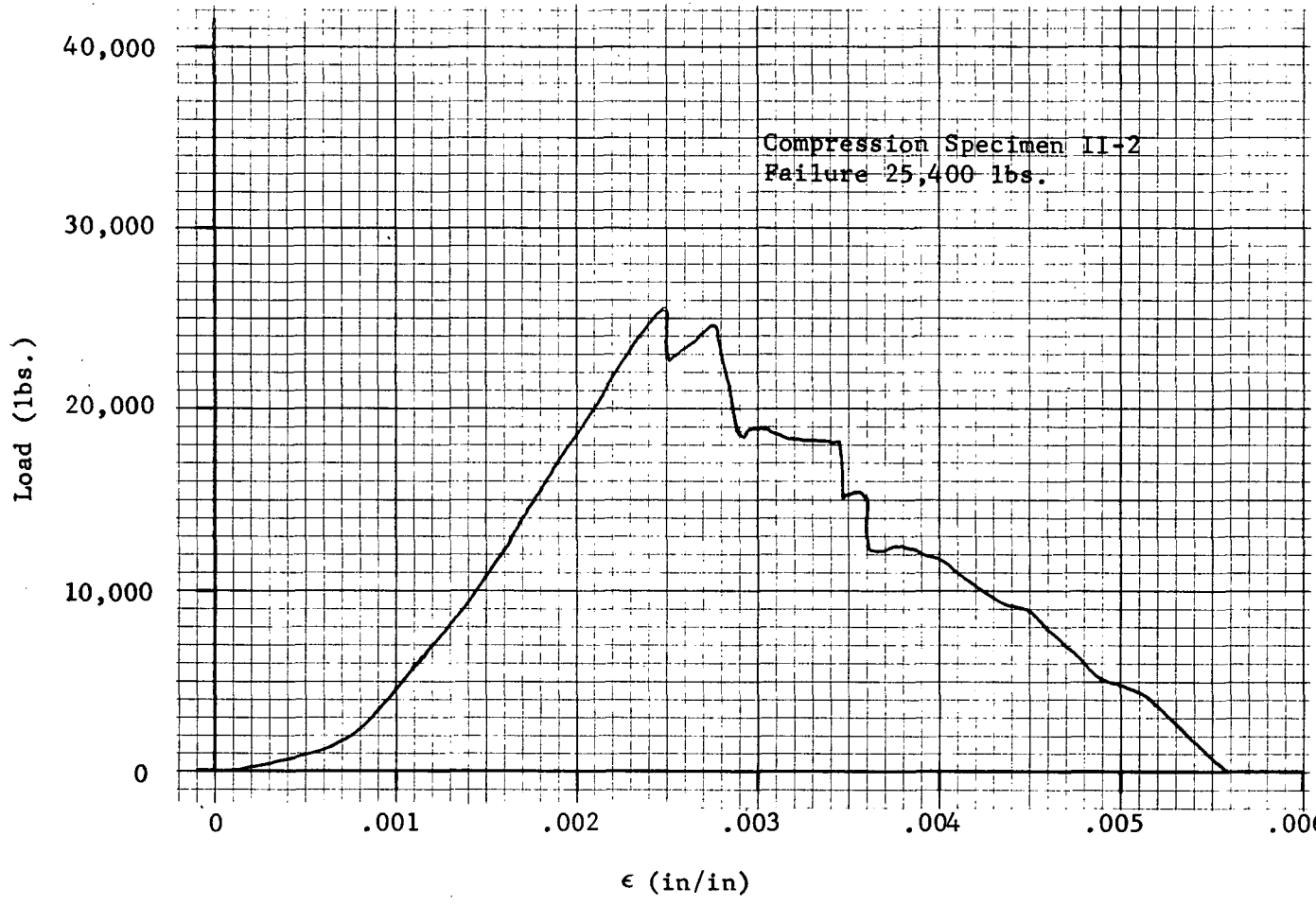

Figure 59. Typical Compression Test.

DISCUSSION OF RESULTS AND RECOMMENDATIONS

The predictions of failure for the compression tests were high if thermal effects were included. The predictions were lower than test values if thermal effects were neglected. Thus it is probable that the effect of thermal prestresses resulting from bonding was overemphasized. The tension test results, as a whole, were closer to prediction. Thermal effects were not expected to affect these results significantly. Additional testing to further evaluate the actual nature of thermal effects is recommended.

The debonding of graphite was the primary cause of complete failure of the compression specimens. This debonding from the crown and skin sections appears to be a post buckling phenomena. Buckling deformation in the aluminum results in failure of the graphite-aluminum bond. The separation of the graphite from the aluminum results in total crippling of the unit. The mechanics of the debonding are not fully explained or understood at this time; however, the incidence of early failure was more prevalent with the thicker graphite reinforcement. Debonding of graphite in tension specimens was primarily limited to the thicker .040 thickness graphite reinforced panels.

Since no all aluminum panels were tested, a direct correlation of efficiencies is not available. However, based on the inclusion of thermal preloads in the total buckling load, very little graphite is necessary to satisfy the requirements of one-third and one-half of the load being carried by the graphite. On the other hand, if the effects of thermal prestresses are minimal, then more graphite is required. This is due to the fact that analytically it is necessary to remove the thermal tension load from the aluminum. Thus, all of the initial compression loading is being carried directly by the graphite. Therefore, at the buckling load the graphite will be carrying a larger portion of the load. Refer to Table VII for a comparison of graphite load carrying capabilities with and without thermal prestresses.

The analysis of the thermal stresses was based on the assumption that the plates would remain flat. Since there was some initial bowing in the panels it follows that the prestresses were not as high as originally predicted.* This is particularly true in the case of the long panels. The long panels (10"x20") suffered premature column and local crippling failure. This failure was attributed to the inability of the potting to eliminate all of the thermal bowing. The bowing of the panel forced premature debonding of the graphite which in turn precipitated local crippling.

*It is also to be noted that the thermal analysis was based on an elastic analysis. An analysis based on a nonlinear adhesive would also reduce the peak thermal stresses.

Thermal stresses seem to be the primary variable of concern with this panel reinforcement concept. It would be desirable to investigate methods of fabrication that would greatly reduce or eliminate their importance. At the present time there appears to be two approaches to the problem: 1. Testing and/or developing suitable room temperature cure adhesives and 2. Utilizing existing approaches and/or developing new procedures to mechanically match the thermal behavior of aluminum and graphite. The latter approach has already been experimented with by Lockheed on the center wing box of the C-130 transport. Whether this approach is viable as a production approach remains to be seen; but, it is definitely worth consideration. The first approach would seem more realistic in terms of production. It is necessary to determine the requirements of an adhesive in the configuration under consideration and then determine if existing room temperature adhesives can meet those requirements or if the development of a satisfactory adhesive is promising.

Another area of concern is the effect of graphite thickness on the stress levels in the adhesive during thermal cycling and on the panel buckling modes. An investigation of this problem is also recommended.

If the problem of thermal stresses and suitable adhesives can be solved, the reinforced stringer concept can easily become a viable production item and a valuable addition to reinforcement concepts.

REFERENCES

1. Needham, R.A.: - The Ultimate Strength of Aluminum Alloy Formed Structural Shapes in Compression. Journal Aerospace Science, Volume 21, April 1954

2. Oeverli, V. and Viswanathan, A.V., BUCLASP - A Computer Program for Uniaxial Compressive Buckling Loads of Orthotropic-Laminated Stiffened Plates, NASA CR 111871

76